European Review for Medical and Pharmacological Sciences 2024; 28: 622-644

Prognostic and immune roles of *UROC1* in human cancers: from mechanism exploration of NAFLD and HCC to pan-cancer analysis

Q.-Y. WANG[1], Y.-J. LIU[1], Y. HU[2], H. XIAO[3], L.-L. XIA[1], Y.-G. WU[4]

[1]Department of Infections Disease, The First Affiliated Hospital of Anhui Medical University, Hefei, Anhui, China
[2]Department of Pathology, Hefei Cancer Hospital, Chinese Academy of Sciences (CAS), Hefei, Anhui, China
[3]Department of Pathology, The First Affiliated Hospital of Anhui Medical University, Hefei, Anhui, China
[4]Department of Nephropathy, the First Affiliated Hospital of Anhui Medical University, Hefei, Anhui, China

Abstract. – OBJECTIVE: Both non-alcoholic fatty liver disease (NAFLD) and hepatocellular carcinoma (HCC) are prevalent diseases worldwide. This study aimed to explore the underlying mechanisms of NAFLD and HCC and identify new therapeutic targets for human cancers.

MATERIALS AND METHODS: NAFLD and HCC gene expression profiles were obtained from the Gene Expression Omnibus (GEO) database. Differentially expressed genes (DEGs) and weighted gene co-expression network analysis (WGCNA) were utilized to identify co-expressed genes associated with NAFLD and HCC. Public databases were consulted to find common targets of NAFLD and HCC. Enrichment analysis and CIBERSORT techniques were employed to analyze the pathways enriched with DEGs and the attributes of infiltrating immune cells. Furthermore, the expression data of *UROC1* and clinical information of patients were acquired from The Cancer Genome Atlas (TCGA) database. Finally, the expression of the *UROC1* was validated by immunohistochemistry (IHC).

RESULTS: Through a comprehensive bioinformatics analysis, eight hub genes (*CCL2, CCR2, IL6, CSF3R, ATL2, SESN3, UROC1, FIGNL1)* were identified. Enrichment analysis indicated that inflammatory and immune response may be common features between NAFLD and HCC. CIBERSORT analysis revealed an imbalance of plasma cells and macrophages in NAFLD and HCC. Pan-cancer analysis demonstrated that *UROC1* expression was related to clinical outcomes and tumor immunity in various cancers. Moreover, a strong correlation was exhibited between *UROC1* expression and crucial elements, including tumor mutation burden (TMB), microsatellite instability (MSI), multiple immune checkpoints (ICP), and tumor microenvironment (TME). Importantly, an adverse clinical prognosis of HCC was linked to decreased *UROC1* expression, which was consistent with IHC results.

CONCLUSIONS: We identified eight hub genes (*CCL2, CCR2, IL6, CSF3R, ATL2, SESN3*, *UROC1*, *FIGNL1*), which may become early diagnostic and therapeutic targets for NAFLD and HCC. The pan-cancer analysis of *UROC1* provides new evidence for its broad application prospects in the field of HCC and other cancers.

Key Words:
NAFLD, HCC, *UROC1*, Bioinformatics, Prognosis, Cancer immunity.

Abbreviations

ATL2: Atlastin GTPase 2; AUC: Area under the curve; *CCL2*: C-C motif chemokine ligand 2; *CCR2*: C-C motif chemokine receptor 2; *CSF3R*: Colony-stimulating factor 3 receptor; CGT: Common gene targets; DEGs: Differentially expressed genes; DGIdb: Drug-gene interaction database; DSS: Disease-specific survival; DFI:Disease-free interval; DC: Dendritic cells; ER:Endoplasmic reticulum; *FIGNL1*: Fidgetin-like 1; GO: Gene Ontology; GEO: Gene expression omnibus; GWAS:Genome-wide association studies; GSEA: Gene set enrichment analysis; *G-CSF*: Granulocyte-colony stimulating factor; HCC: Hepatocellular carcinoma; HGs: Hub genes; HSCs: Hepatic stellate cells; IHC: immunohistochemistry; ICP: Immune check- points; *IL-6*: Interleukin-6; *JAK2*: Janus kinase 2; KCs: Kupffer cells; KEGG: Kyoto Encyclopedia of Genes and Genomes; LSECs: Liver sinusoidal endothelial cells; MSI: Microsatellite instability; NKs: Natural killer cells; OS: Overall survival; PPI: Protein-protein interaction; PFI: progression-free interval; *RIG-I*: Retinoic acid-inducible gene I; ROC: Receiver operating characteristic; NAFLD: Nonalcoholic fatty liver disease; NASH: Nonalcoholic steatohepatitis; TCGA: The Cancer Genome Atlas;

Corresponding Authors: Lingling Xia, MD; e-mail: 13966684365@163.com; yzb@ahmu.edu.cn; Yonggui Wu, MD; e-mail: wuyonggui@medmail.com.cn

TMB: Tumor mutation burden; TME: Tumor microenvironment; *TGF-beta*: Transforming growth factor-beta; *TNF*: Tumor necrosis factor; *TLR*: Toll-like receptor; *SESN3*: Sestrin 3; *STAT3*: Signal transducer and activator of transcription-3; *UROC1*: Urocanase domain containing protein 1; WGCNA: Weighted gene co-expression network analysis.

Introduction

Non-alcoholic fatty liver disease (NAFLD) is caused by metabolic syndrome, and its association with hepatocellular carcinoma (HCC) has been established[1,2]. It is predicted that the prevalence of nonalcoholic steatohepatitis (NASH) will increase by 56% from 2016 to 2030 in countries such as the United States, Europe, and China[3]. Moreover, NAFLD has become a cause of HCC with the highest rate of growth in the United States, the United Kingdom, and France[4]. Therefore, alleviating the burden of NAFLD-related HCC is urgent. HCC accounts for more than 80% of primary liver cancers worldwide[5] and is the fourth leading cause of cancer-related death globally[6]. There are several factors for HCC, including chronic hepatitis, alcohol, metabolic liver diseases (especially NAFLD), and medications[7], while NAFLD-related HCC is often delayed in treatment due to a lack of symptoms, resulting in lower survival rates[8,9]. Therefore, exploring new pathways and genes that regulate NAFLD/HCC through bioinformatics and public databases is of great significance.

Over the past few years, the introduction of high-throughput technology and bioinformatics analysis has enabled the identification of pathogenic genes in carcinogenesis and a deeper understanding of disease pathophysiology[10]. Multiple bioinformatics studies in the literature have provided new insights into potential targets for NAFLD and HCC. Genome-wide association studies (GWAS) have revealed that several genes, including *TM6SF2*, *ENPP1*, *IRS-1*, and *FATP5*, are related to the development of NAFLD[11]. Another investigation[12] identified promising gene objectives that possess a correlation with the incidence of NAFLD and HCC. Cai et al[13] found that the new gene *CEP192* is an essential factor in the progression of NAFLD into HCC, but further experimental verification is needed. Although there is convincing evidence[14] of a link between HCC and NAFLD, their underlying molecular mechanisms remain elusive, and no drugs have been approved for the treatment of NAFLD/NASH.

Therefore, this research was carried out to integrate and analyze gene data from NAFLD and HCC patients in public databases, screen for hub genes (HGs), and explore the potential biological and immunological mechanisms. Additionally, a new gene (*UROC1*) was selected, and pan-cancer analysis was conducted to identify novel and promising targets for the treatment of tumor patients. The current research workflow is illustrated in Figure 1.

Materials and Methods

Online Data Acquisition

The microarray data were downloaded from the Gene Expression Omnibus (GEO) database (http://www.ncbi.nlm.nih.gov/geo/). Relevant gene expression datasets for 'NAFLD' and 'HCC' keywords were examined, leading to the acquisition of datasets GSE63067, GSE89632, GSE58979, GSE19665, GSE41804, and GSE46408 with corresponding accession numbers. Commonly co-expressed genes between NAFLD and HCC were identified from the Comparative Toxicogenomics Database (CTD; http://ctdbase.org/)[15], GeneCards (http://www.GeneCards.org/)[16], and DisGeNET (http://www.disgenet.org/)[17], a comprehensive platform that integrates human disease-related genes and variation information.

The Cancer Genome Atlas (TCGA, https://portal.gdc.cancer.gov/)[18] encompassed more than 20,000 primary cancers across 33 cancer types, along with their corresponding normal tissues, examined at the molecular level. We downloaded TCGA transcriptome RNA-seq data and clinical information from UCSC Xena (http://xena.ucsc.edu/)[19]. Additionally, we collected clinical information about HCC patients from TCGA, namely, pathological stage, survival time, and survival status for subsequent analysis.

Identification of DEGs

To examine the differentially expressed genes (DEGs), we employed the "limma" package in the R software[20]. By comparing the gene expression profiles of the disease group and the control group, we identified the DEGs within the GSE19665 and GSE89632 datasets and p-value < 0.05 indicated statistical significance. A Venn diagram was used to obtain the common DEGs, and volcanic maps and ridge maps were drawn using the "heatmap" package and the "string" package, respectively.

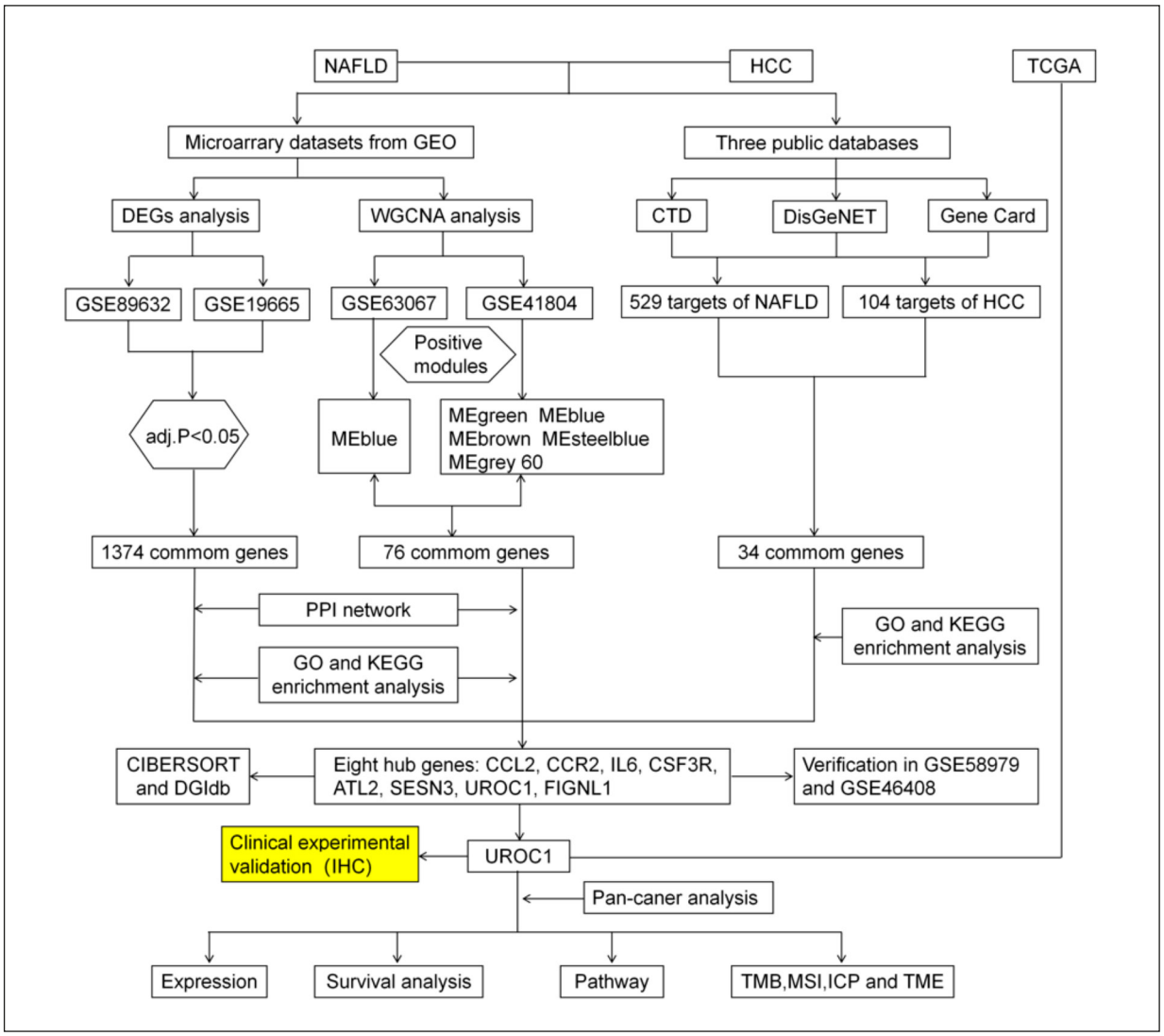

Figure 1. Research design flow chart.

Enrichment Analysis

The "clusterProfiler" package of the R software[21] was utilized for GO and KEGG enrichment analysis, and a p-value < 0.05 was taken as the screening criterion. Histograms and bubble charts were generated through the package "ggplot2" of the R software. In addition, gene set enrichment analysis (GSEA) was conducted using the "clusterProfiler" package to explore the biological pathways of *UROC1* in pan-cancer.

PPI Network Construction

The construction of the PPI network was accomplished by utilizing the STRING database (http://string-db.org/)[22], which predicts protein functional associations. The integrated regulatory network was visualized using Cytoscape software[23], and the top ten genes were determined through the CytoHubba plugin.

WGCNA

Weighted gene co-expression network analysis (WGCNA) is a method used to analyze gene modules that have remarkable biological relevance[24]. The "WGCNA" package in R software was adopted to explore the GSE63067 and GSE41804 datasets to identify modules related to NAFLD and HCC. Based on the standard of $R^2 = 0.9$, we calculated a proper soft threshold power β (ranging from 1 to 30). Subsequently, a hierarchical clustering was employed to obtain a hierarchical clustering tree.

A minimum of 50 genes were set for each module, and modules with a correlation exceeding 50% were merged for a second time. Module eigengenes were identified, and their association with clinical features was computed to generate the expression profiles of all modules. Subsequently, our research focused on the modules that showed a high correlation coefficient with clinical features. Further analysis was then performed using the genes selected from these modules.

WGCNA Analysis of Gene Modules

We determined the key modules for NAFLD and HCC by using Pearson's correlation coefficients, *p*-values of feature genes, and disease features in each module. Then, shared genes were obtained from the key modules using ImageGP[25].

Common Targets

Common NAFLD- and HCC-related genes shared among the CTD, DisGeNET, and GeneCards databases were identified using Venn diagrams. Then, the common gene targets (CGT) of NAFLD and HCC were determined by finding the intersection of these genes.

Hub Genes Selection and Validation

CGT of NAFLD and HCC were obtained from public disease databases, and the hub genes (HGs) were identified through the intersection of WGCNA and DEG results. We validated their expression in GSE58979 and GSE46408. A *t*-test was conducted to handle the data of two groups, with p-value < 0.05 indicating statistical significance.

Immune Infiltration

CIBERSORT (https://cibersortx.stanford.edu/) is an algorithm that allows for the estimation of cell type abundances in mixed cell populations[26]. We determined immune cell infiltration using the CIBERSORT, with the reference set of 22 immune cell genes (LM22) and a permutation number of 1,000. Then, we retained a p-value < 0.05 in the CIBERSORT results and calculated the correlation among various immune cells using the Spearman analysis. The "corrplot" and "vioplot" packages in R software were adopted to perform correlation analysis and visualization.

DGIdb

The Drug-Gene Interaction Database (DGIdb, http://www.dgidb.org/) is a valuable resource for finding gene-drug interactions and potential therapeutic drugs[27]. We accessed the DGIdb website to gather potential drugs and their interactions with HGs.

Expression Analysis of UROC1 in Pan-Cancer

The exploration of *UROC1* expression dysregulation in various cancer types and normal tissues was conducted by analyzing data obtained from TCGA. The RNA sequencing data and clinical follow-up data were obtained from 33 types of cancer, including adrenocortical carcinoma (ACC), thyroid carcinoma (THCA), breast invasive carcinoma (BRCA), liver hepatocellular carcinoma (LIHC), uterine carcinosarcoma (UCS), cervical squamous cell carcinoma and endocervical adenocarcinoma (CESC), colon adenocarcinoma (COAD), uterine corpus endometrial carcinoma (UCEC), diffuse large B-cell lymphoma (DLBC), esophageal carcinoma (ESCA), glioblastoma multiforme (GBM), low-grade glioma (LGG), bladder urothelial carcinoma (BLCA), head and neck squamous cell carcinoma (HNSC), kidney chromophobe (KICH), cholangiocarcinoma (CHOL), kidney renal papillary cell carcinoma (KIRP), acute myeloid leukemia (AML), lung adenocarcinoma (LUAD), sarcoma (SARC), lung squamous cell carcinoma (LUSC), mesothelioma (MESO), pheochromocytoma and paraganglioma (PCPG), prostate adenocarcinoma (PRAD), ovarian serous cystadenocarcinoma (OV), rectum adenocarcinoma (READ), skin cutaneous melanoma (SKCM), stomach adenocarcinoma (STAD), testicular germ cell tumors (TGCT), pancreatic adenocarcinoma (PAAD), thymoma (THYM), kidney renal clear cell carcinoma (KIRC), and uveal melanoma (UVM) from TCGA. The "Wilcox" test was employed to evaluate the expression levels of HGs in cancer tissues *vs.* normal tissues.

Prognostic Analysis

We examined whether there is a connection between the expression of *UROC1* in individuals with cancer and clinical outcomes, such as overall survival (OS), progression-free interval (PFI), disease-specific survival (DSS), and disease-free interval (DFI), with forest plots and Kaplan-Meier curves. In addition, we calculated Hazard ratios and 95% confidence intervals through multivariate analysis of survival. The "survival" and "survminer" packages in R software were used for survival analysis of HGs in pan-cancer, and the package "forestplot" in R software was used for visualization.

Pan-cancer Relationships Between UROC1 and Immune Characteristics

The tumor microenvironment (TME) is made up of immune and stromal components. We analyzed the correlation between the scores for immune and stromal components and the levels of *UROC1* expression using the "estimate" and "limma" R packages. Spearman's analysis was utilized to examine the relationship between *UROC1* expression and tumor mutation burden (TMB) or microsatellite instability (MSI) and represented the results using radar plots created with the 'fmsb' R package. Furthermore, we investigated whether there is a link between *UROC1* expression and immune checkpoints (ICP) in human cancers. Differences were considered significant if the p-value < 0.05.

Clinical Samples

Liver cancer tissues and their paracancerous tissues were acquired from a group of twenty patients at the First Affiliated Hospital of Anhui Medical University. None of the HCC patients had systemic antitumor treatment before surgery. This study was approved by the Ethics Committee of the First Affiliated Hospital of Anhui Medical University (Ethical Approval No. PJ2023-06-33).

Immunohistochemistry

For immunohistochemistry (IHC), the sections were incubated overnight at 4°C with anti-*UROC1* antibodies (1:20, Thermo Fisher Scientific, Waltham, MA, USA). Afterward, appropriate secondary antibodies were applied for an additional 30 minutes at 37°C. Finally, the slides were imaged using a microscope.

Statistical Analysis

All statistical data were analyzed using R software version 4.2.3, and $p < 0.05$ was regarded as statistically significant.

Results

GEO Information

We selected a total of six GEO datasets (GSE63067, GSE89632, GSE58979, GSE19665, GSE41804, and GSE46408). Detailed information on these six datasets, such as GSE number, sample, and detection platform, is presented in Table I. For DEG analysis, GSE89632 and GSE19665 were paired; for WGCNA analysis, GSE63067 and GSE41804 were paired; and for the validation of the expression levels of HGs, GSE58979 and GSE46408 were adopted.

Identification of DEGs

GSE89632 included 24 NAFLD tissue samples from humans and 19 normal liver tissue control samples, while the GSE19665 dataset included 10 HCC tissue samples and 10 normal control samples. According to the differential analysis using R software, we identified 408 and 2,060 DEGs in GSE89632 and GSE19665, respectively. The heatmap and volcanic map display the overall distribution of DEGs with a fold change > 1 and an adj. p-value < 0.05 (Figure 2A-D). Functional enrichment analysis using GSEA was performed on DEGs with a p-value < 0.05. Common DEGs in NAFLD were enriched in inflammatory and immune response signaling pathways, such as the interleukin (IL)-17 pathway, *nuclear factor (NF)-kappa B* pathway, *Janus kinase/signal transducers and activators of transcription (JAK/STAT)* pathway, *advanced glycation end product (AGE)-receptor for AGE (RAGE)* pathway, and *tumor necrosis factor (TNF)* pathway. Similarly, common DEGs in HCC were also enriched in signaling pathways, including *JAK-STAT, TNF*, and *NF-kappa B*, and played important roles in the differentiation of Th17 cell, Th1, and Th2 cells (Figure 2E-F), indicating that inflammation and immunity may be common biological mechanisms underlying NAFLD and HCC.

Table I. Detailed information of GEO datasets.

ID	GSE number	Platform	Samples	Disease
1	GSE63067	GPL570	7 controls and 9 patients	NAFLD
2	GSE89632	GPL14951	24 controls and 19 patients	NAFLD
3	GSE58979	GPL15207	27 controls and 25 patients	NAFLD
4	GSE19665	GPL570	10 controls and10 patients	HCC
5	GSE41804	GPL570	20 controls and 20 patients	HCC
6	GSE46408	GPL4133	6 controls and 6 patients	HCC

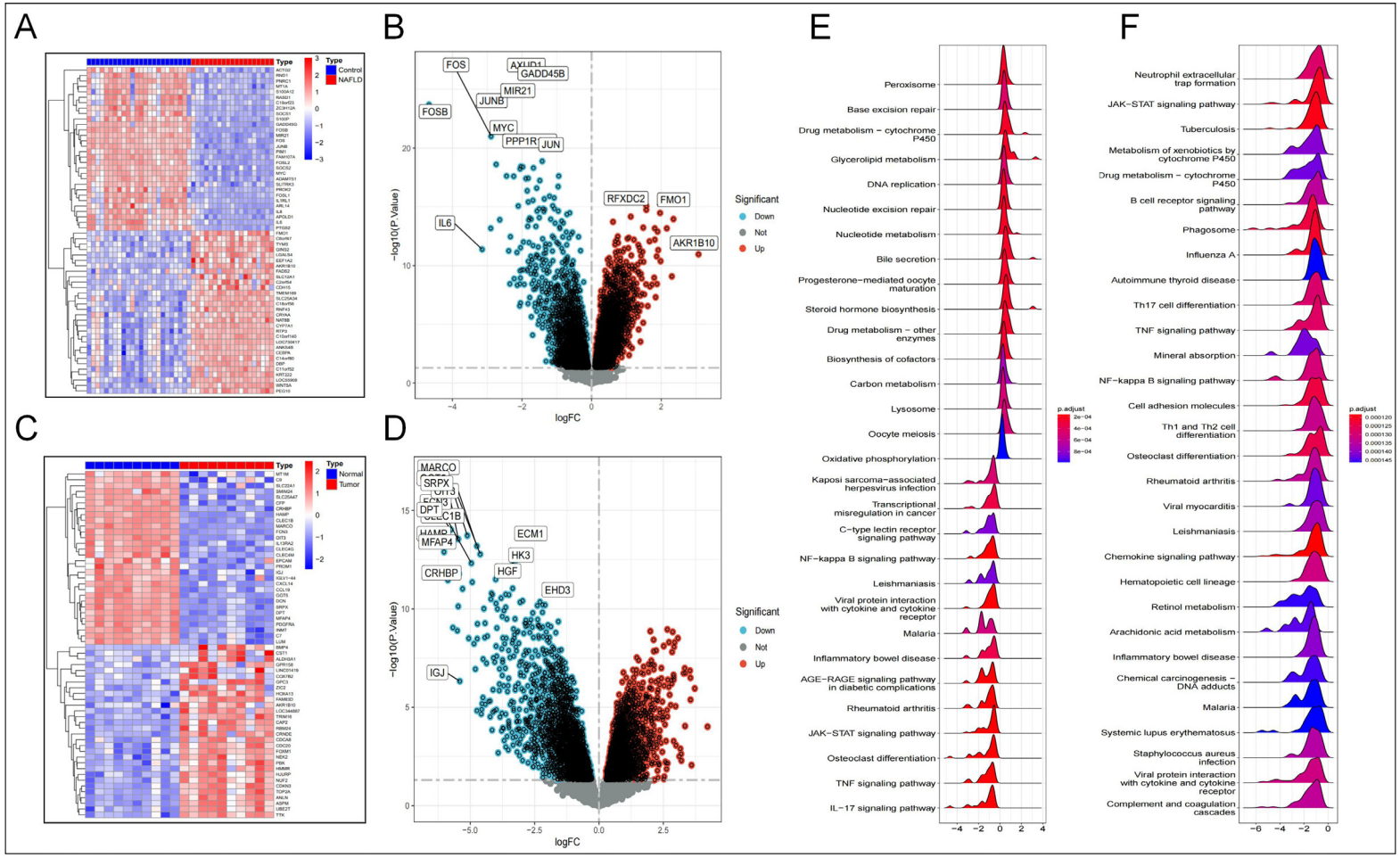

Figure 2. Identification of DEGs among NAFLD and HCC. **A**, Heatmap of overlapping DEGs in GSE89632. **B**, Volcanic map of overlapping DEGs in GSE89632. **C**, Heatmap of overlapping DEGs in GSE19665. **D**, Volcanic map of overlapping DEGs in GSE19665. **E**, GSEA analysis of DEGs in GSE89632. **F**, GSEA analysis of DEGs in GSE19665.

Subsequently, 1,374 co-expressed genes were acquired through the public platform Venn diagram network (http://bioinformatics.psb.ugent.be/webtools/Venn/) (Figure 3A). A Protein-Protein interaction (PPI) network for DEGs was established with the STRING database (**Supplementary Figure 1**), including 1,369 nodes and 1,905 edges. Next, the network was visualized using Cytoscape, and the top ten HGs were screened out with the cytoHubba (Figure 3B). According to GO analysis, the 1,374 DEGs were involved in such biological processes as immune receptor activity, cytokine receptor activity, and *transforming growth factor-beta (TGF-beta)* binding (Figure 3C). KEGG analysis illustrated that DEGs were concentrated not only in oncogenic pathways such as transcriptional misregulation in cancer, DNA replication, and Cell cycle but also in human T-cell leukemia virus 1 (HTLV-1) infection and differentiation of Th17 cell (Figure 3D). These findings were consistent with the results described above.

WGCNA

By conducting WGCNA analysis on the GSE63067 dataset of NAFLD, we selected the appropriate soft threshold (β) to construct the network (Figure 4A). The resulting cluster dendrogram was then drawn to visualize the modules represented by different colors (Figure 4B). Based on the criteria of a correlation coefficient > 0.5 and a *p*-value < 0.05, we found that the MEblue module (r = 0.53, $p = 0.04$) was highly correlated with NAFLD, as shown in Figure 4C. We further analyzed the genes in the MEblue module, which included 222 genes, as shown in Figure 4D.

Similarly, WGCNA analysis of the GSE41804 dataset was performed to obtain hierarchical clustering trees and expression modules (Figure

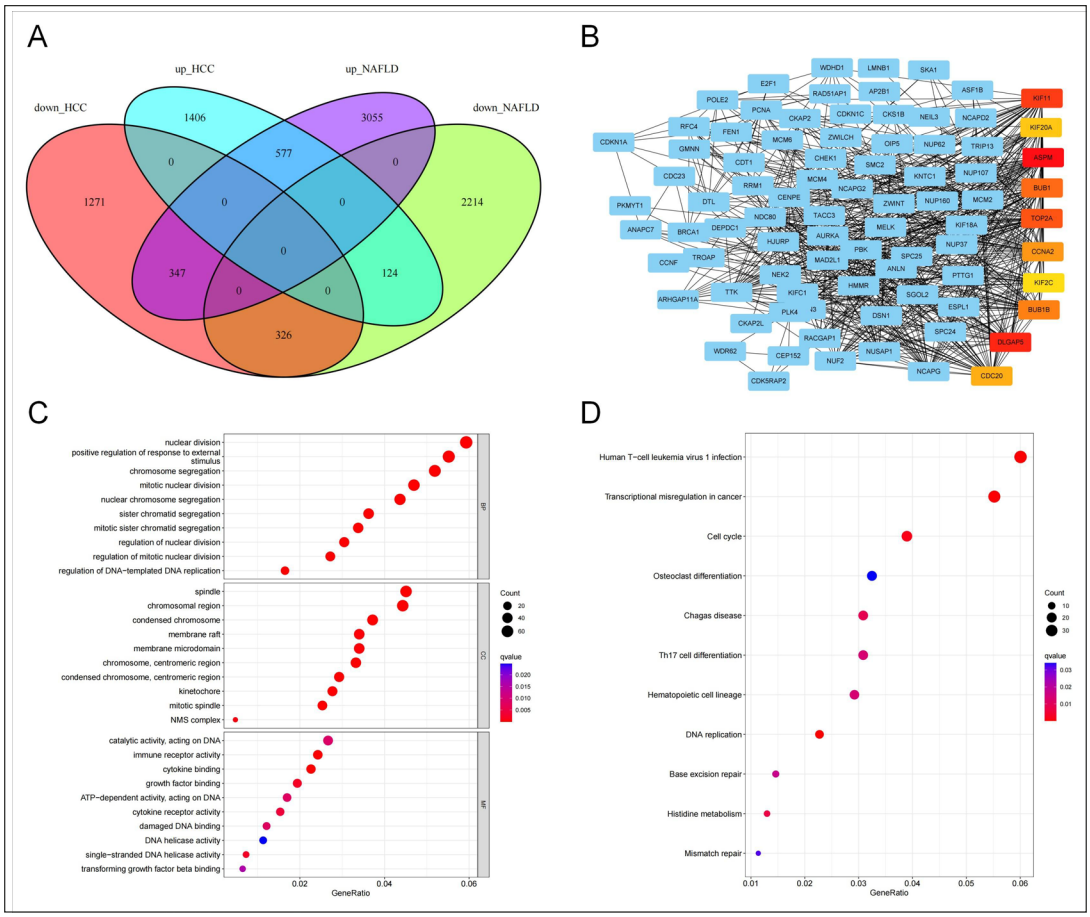

Figure 3. Analysis of common DEGs between NAFLD and HCC. **A**, Venn diagram showing the overlaps of numbers of DEGs between two selected GEO datasets. **B**, PPI network of DEGs. **C**, GO enrichment analysis of DEGs. **D**, KEGG enrichment analysis of DEGs.

5A-B). Among these 21 modules, five modules, including "MEgreen", "MEblue", "MEbrown", "MEgrey 60", and "MEsteelblue", were positively correlated with HCC (MEgreen: r = 0.6, p = 4e-05; MEblue: r = 0.55, p = 2e-04; MEbrown: r = 0.68, p = 1e-06; MEgrey 60: r = 0.78, p = 4e-09; MEsteelblue: r = 0.59, p = 6e-05), comprising 2,120, 1,577, 4,021, 3,184, 219, and 87 genes, respectively (Figure 5C-H).

Enrichment Analysis of Common Genes Recognized by WGCNA

There were 76 common genes identified within the NAFLD-related module and HCC-related modules (**Supplementary Figure 2A**). A PPI network was composed of 101 nodes and 14 edges (**Supplementary Figure 2B**). Enrichment analysis unveiled that these genes predominantly functioned in various biological activities, such as desmosome organization, axonal growth cone, ATPase-coupled ion transmembrane transporter activity, and Human papillomavirus infection (**Supplementary Figure 2C-D**).

Analysis of Common Gene Targets in Public Databases

For the integration of the biological data that have been reported, we used Venn diagram software to combine NAFLD- and HCC-related genes from the CTD, DisGeNET, and GeneCards databases. We selected 529 genes in relation to NAFLD and 104 genes related to HCC, yielding 34 common gene targets between NAFLD and HCC (Figure 6A-C). According to the GO analysis of these 34 common genes, they were involved in RNA regulation, signaling receptor activator activity, protein

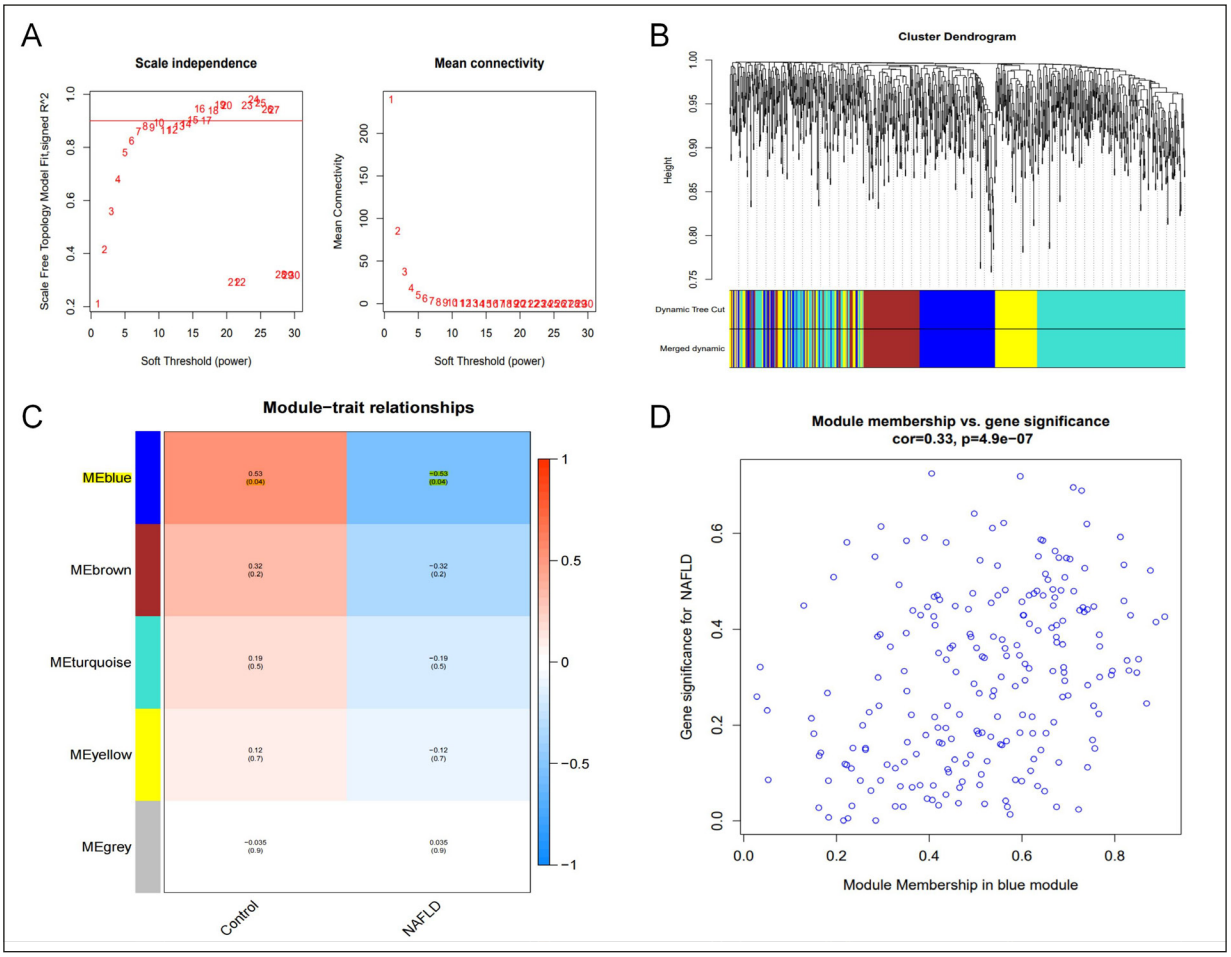

Figure 4. WGCNA of GSE63067 dataset. **A**, Soft threshold analysis in NAFLD. **B**, Module correlations in NAFLD. **C**, Heatmap of the module-trait relationship in NAFLD. Each cell contains the corresponding correlation and p-value. **D**, Module membership in the blue module in NAFLD.

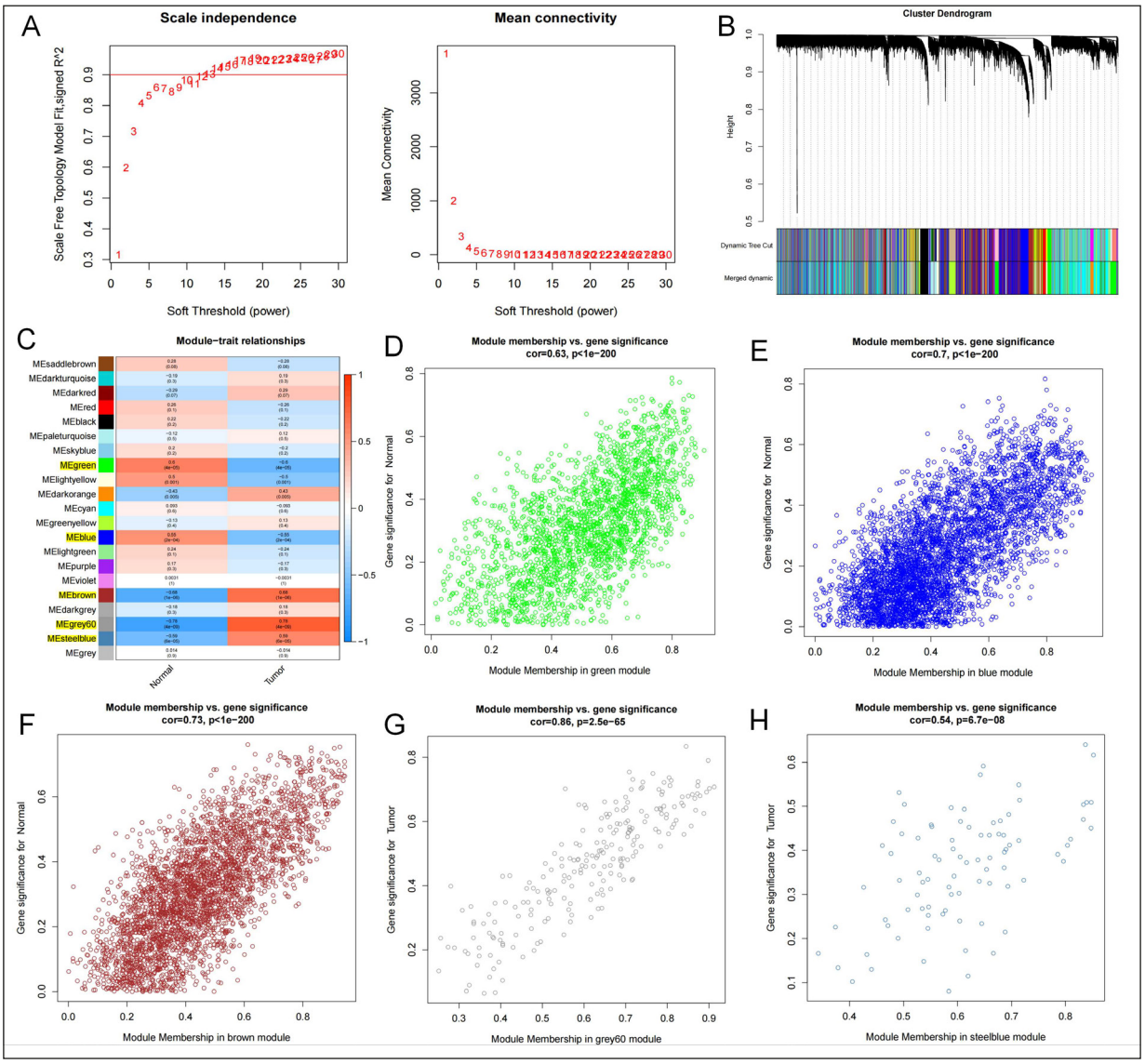

Figure 5. WGCNA of GSE41804 dataset. **A**, Soft threshold analysis in HCC. **B**, Module correlations in HCC. **C**, Heatmap of the module-trait relationship in HCC. Each cell contains the corresponding correlation and *p*-value. **D-H**, Module membership in selected modules in HCC.

phosphatase binding, and other biological processes (Figure 6D). KEGG analysis indicated that these genes were connected to various metabolic pathways, such as *Mitogen-activated protein kinase (MAPK)* signaling pathway, hypoxia-inducible factor-1 (HIF-1), Phosphatidy-Linositol 3-kinase (PI3K)/protein kinase B (PKB/AKT), AGE-RAGE in diabetic complications, and *TNF* pathway (Figure 6E). These results further validate the role of inflammation and immune pathways in NAFLD and HCC.

Identification and Analysis of HGs

After intersecting the above data in the three result sets, we identified eight HGs (*CCL2*, *CCR2*, *IL6*, *CSF3R*, *ATL2*, *SESN3*, *UROC1*, *FIGNL1*), as illustrated in Figure 7A. To validate the expression levels of these HGs, we detected their expression in NAFLD using the GSE58979 dataset and in HCC using the GSE46408 dataset. Interestingly, only *FIGNL1* was upregulated in NAFLD, while *CCL2*, *IL6*, *CSF3R*, and *UROC1* were all downregulated. In HCC, *FIGNL1* and *ALT2*

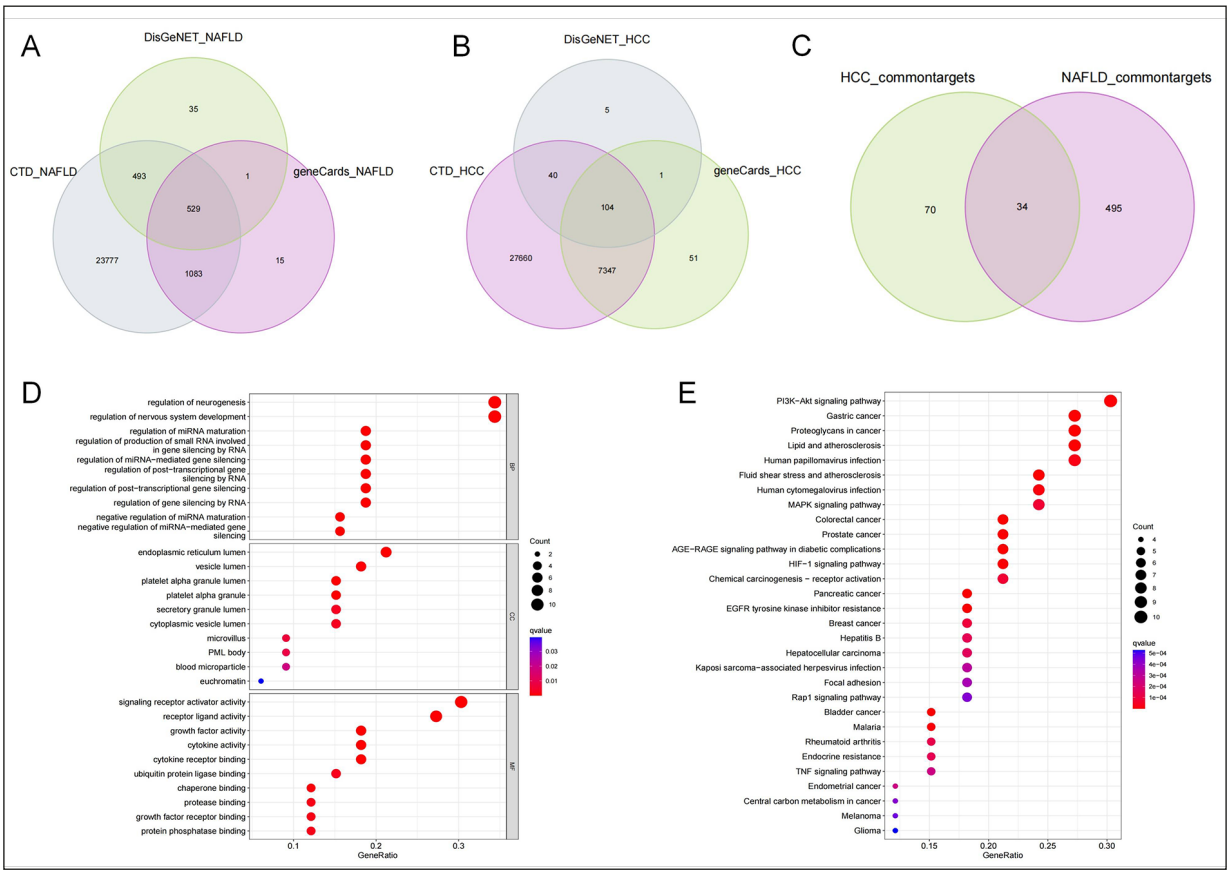

Figure 6. Analysis of common targets between NAFLD and HCC from three public databases. **A-C**, Venn diagram of common targets between NAFLD and HCC. **D**, GO enrichment analysis of the common targets. **E**, KEGG enrichment analysis of the common targets.

remained upregulated, while *UROC1* showed a consistent trend of downregulation as in NAFLD (Figure 7B-C). Moreover, the "survival ROC" software tool was employed to generate receiver operating characteristic (ROC) curves, where the horizontal and vertical axes corresponded to the false-positive rate and true-positive rate, respectively. A larger area under the ROC curve (AUC) indicated a higher predictive accuracy. The results indicated that the AUCs of these biomarkers in both NAFLD and HCC were higher than 0.75, indicating that the diagnostic capability of these biomarkers was high (Figure 7D-E). Notably, *UROC1* and *FIGNL1* had an AUC of 1 in HCC, and both also showed good diagnostic values in NAFLD, which caught our attention.

Immune Cell Infiltration

The immune cell infiltration analysis was performed with the GSE89632 and GSE19665 datasets. Both NAFLD and HCC had a lower percentage of plasma cells ($p < 0.001$, $p = 0.001$) and a higher percentage of γδT cells ($p < 0.001$, $p = 0.031$) than the normal tissues. NAFLD had significantly higher proportions of both M1 macrophages ($p = 0.034$) and M2 macrophages ($p < 0.001$) than the normal tissues, while HCC had a higher proportion of M0 macrophages ($p = 0.029$) than the normal tissues (Figure 8A-B). Next, the correlation analysis was conducted for the HGs and infiltrating immune cells. As can be seen in Figure 8C for NAFLD, *UROC1* has a positive correlation with resting mast cells (MCs) ($p < 0.05$), while *SESN3* has a negative correlation with activated CD4 memory T cells ($p < 0.01$) and CD8 T cells ($p < 0.05$). *IL6* had a negative relationship with naive B cells ($p < 0.05$) and a positive relationship with resting dendritic cells ($p < 0.05$), while *CCR2* had a negative relationship with resting DCs and M2 macrophages ($p < 0.01$ for both). *CCL2* had a positive relationship with M1 macrophages ($p < 0.01$) and resting CD4

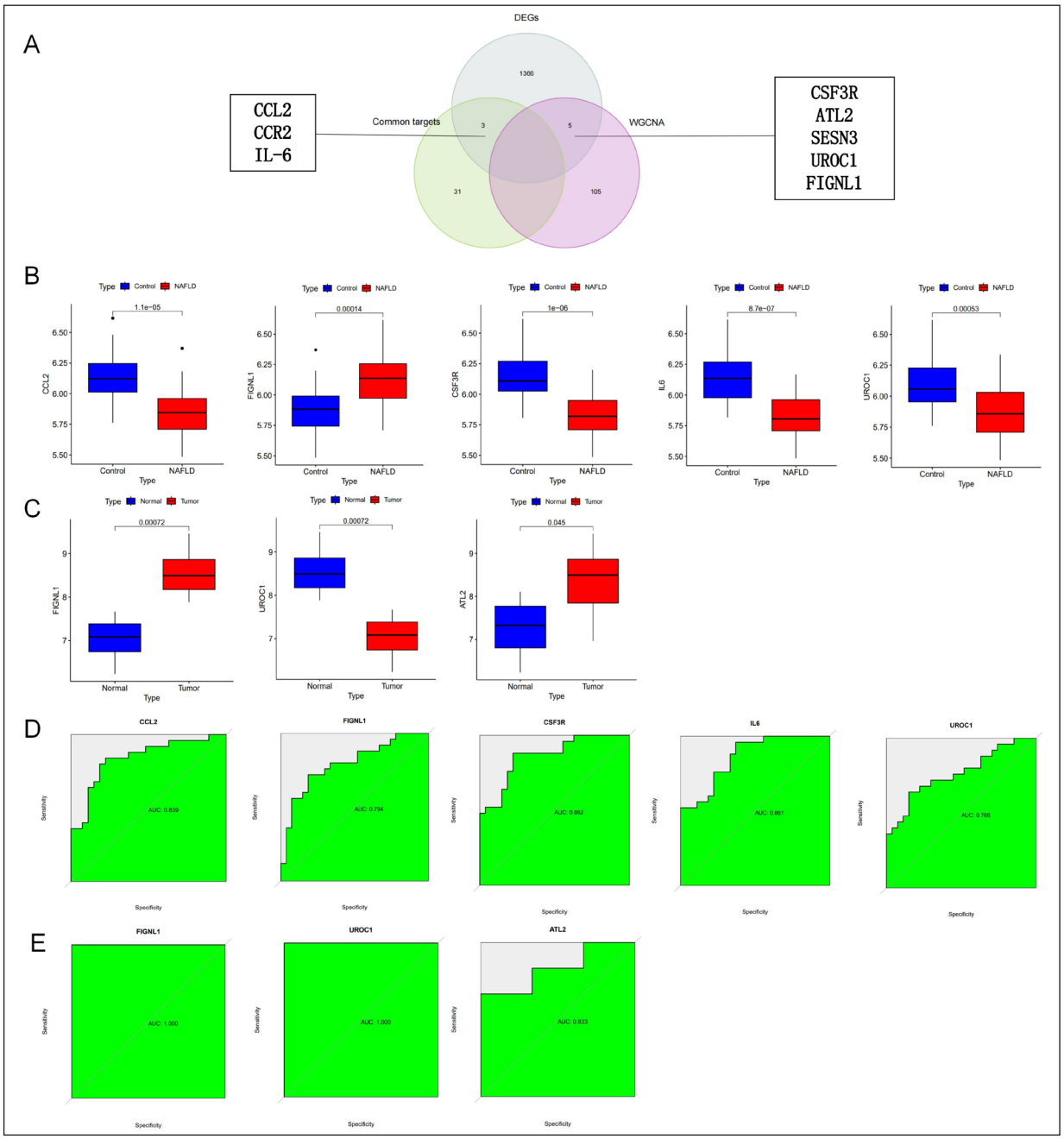

Figure 7. Identification and verification of hub genes. **A**, Venn diagram of common targets and genes from WGCNA and DEGs analysis. **B**, The expression level of hub genes in GSE58979. **C**, The expression level of hub genes in GSE46408. **D**, ROC of hub genes in GSE58979. **E**, ROC of hub genes in GSE46408.

memory T cells ($p < 0.05$), and a negative relationship with M2 macrophages and CD8 T cells ($p < 0.05$ for both).

In HCC (Figure 8D), *SESN3* was positively correlated with CD8 T cells ($p < 0.01$), while *IL6* was negatively related to monocytes ($p < 0.05$) and positively related to γδT cells ($p < 0.05$). *FIGNL1* had a positive association with plasma cells ($p < 0.05$), while *CCR2* was positively correlated with naive B cells ($p < 0.01$) and CD8 T cells ($p < 0.05$) and a negative correlation with activated MCs ($p < 0.05$). *ATL2* had a negative correlation with resting DCs ($p < 0.05$) and neutrophils ($p < 0.01$).

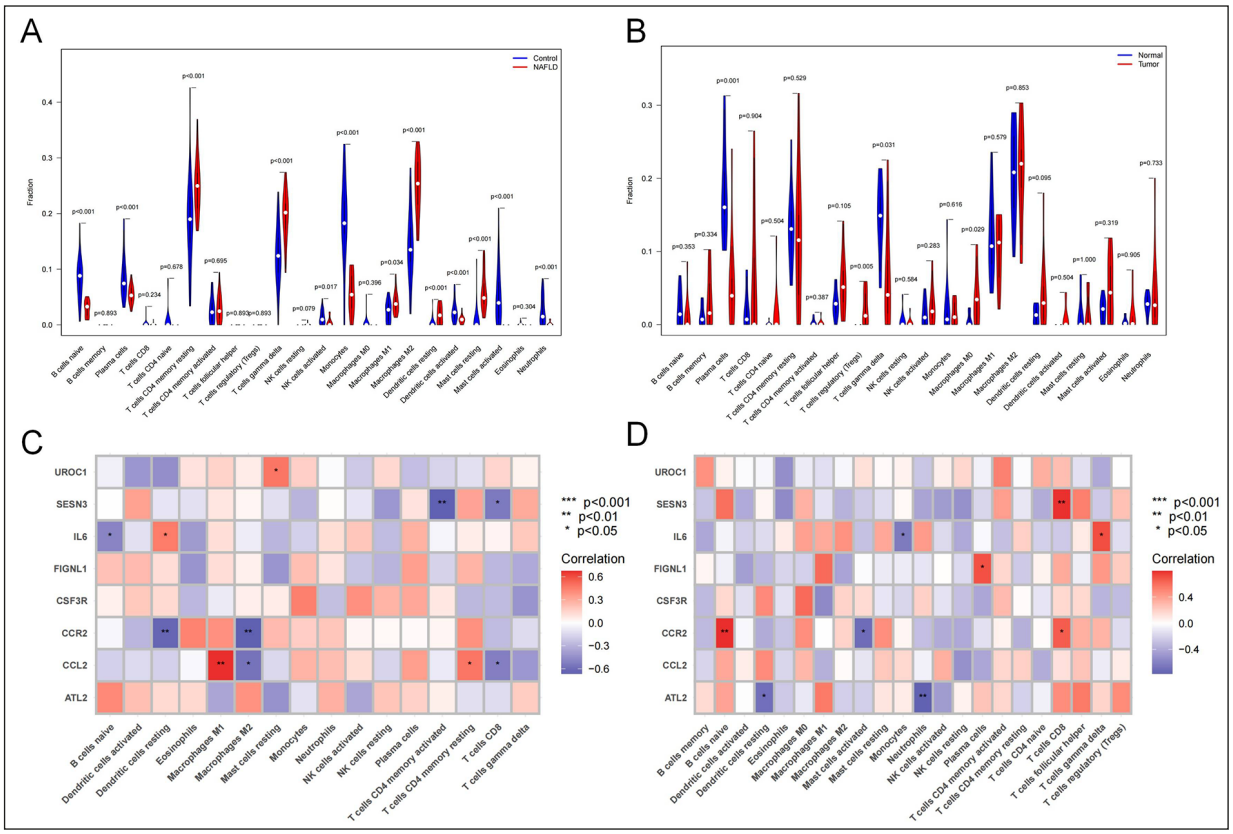

Figure 8. Distribution and visualization of immune cell infiltration. **A**, Comparison of 22 immune cell subtypes between NAFLD tissues and normal tissues. **B**, Comparison of 22 immune cell subtypes between HCC tissues and normal tissues. **C**, Correlation between hub genes and infiltrating immune cells in NAFLD. **D**, Correlation between hub genes and infiltrating immune cells in HCC. *$p < 0.05$, **$p < 0.01$, and ***$p < 0.001$.

Drug-Gene Interactions or Potential Drug Categories

We used the DGIdb database of gene-drug interactions to find prospective therapeutic drugs and the interactions of *CCR2*, *IL6*, *CCL2*, and *CSF3R* with drugs are shown in **Supplementary Figure 3**.

Pan-Cancer Expression of UROC1

Based on the results, we focused on *UROC1* and *FIGNL1*. Previous pan-cancer reports[28] have demonstrated the role of *FIGNL1* in HCC and other tumors, so we selected *UROC1* for preliminary pan-cancer analysis. We compared *UROC1* expression in various cancers using data from TCGA. In the COAD, STAD, HNSC, KIRC, KIRP, READ, PAAD, PCPG, and UCEC, *UROC1* was upregulated. However, *UROC1* was significantly downregulated in both LIHC and CHOL (Figure 9).

The Correlation of UROC1 Expression with Clinical Pathological Features

To assess the correlation of *UROC1* expression and various clinical pathological stages in different cancers, we evaluated *UROC1* expression in patients with cancer at stages I to IV. According to the results obtained from the TCGA, the differential expression of *UROC1* between stages I and II and stages I and III tumor tissues was significant in both LIHC and TGCT. In KIRC, the differential expression of UROCI between stages I and IV, as well as stages I and II, were also significant. In KICH, only the differential expression of *UROC1* between stage I and II patients' tumor tissues was statistically significant. In ESCA, SKCM, and BRCA, only stage II and III tumor tissues showed differential expression of *UROC1*. However, the expression of *UROC1* in LUAD was only associated with pathological stages I and III (Figure 10). In the remaining cancer samples, there was

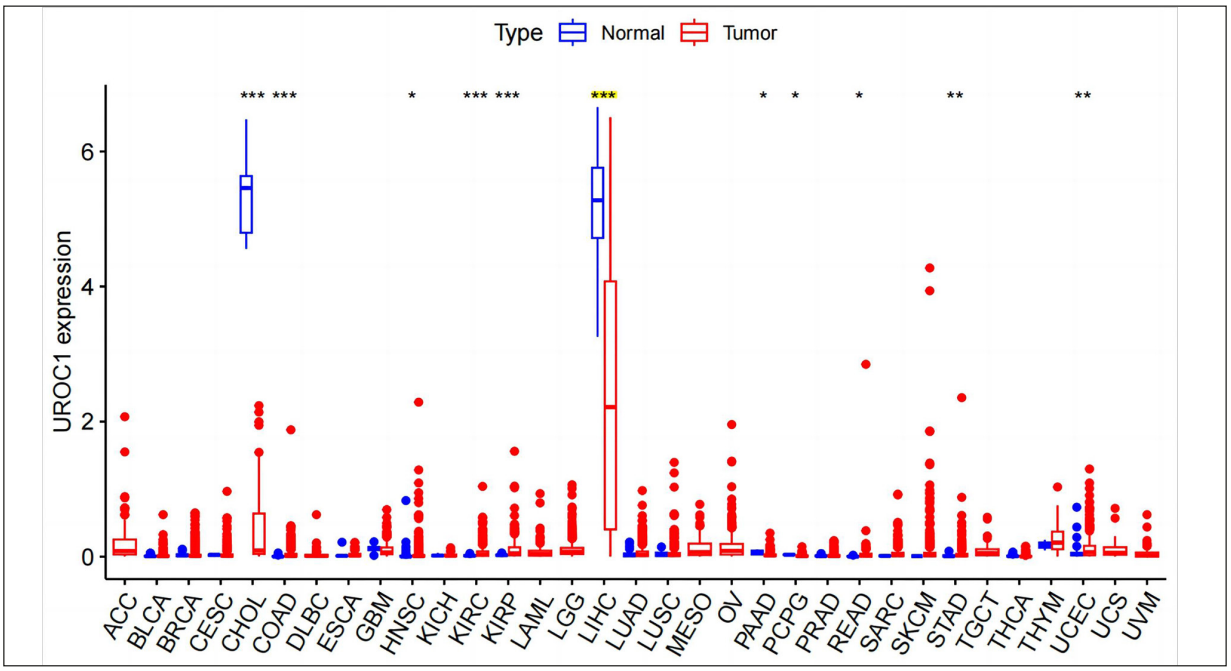

Figure 9. The expression level of *UROC1* in different cancer types from TCGA. *$p < 0.05$, **$p < 0.01$, and ***$p < 0.001$.

no significant correlation between *UROC1* and the patient's pathological stage.

Analysis of the Multi-Faceted Prognostic Value of UROC1 in Pan-Cancer

We evaluated the correlation between patient prognosis and *UROC1* expression in a pan-cancer dataset. The survival indicators included OS, DSS, PFI, and DFI. It can be seen from the Kaplan-Meier survival curves that *UROC1* expression has a significant relationship with OS in KIRC, LIHC, THCA, LAML, and THYM (Figure 11A-E). According to the multivariable Cox regression analysis of 33 types of cancer, *UROC1* expression served as an independent prognostic indicator for OS in DLBC, KIRC, LAML, LIHC, SKCM, and THYM (Figure 11F).

We further determined the correlation between *UROC1* expression and DSS in individuals with cancer. Kaplan-Meier analysis indicated a correlation of *UROC1* expression with DSS in patients with KIRC and LUAD (**Supplementary Figure 4A**). Moreover, we analyzed the effects of *UROC1* expression on DFI and PFI in cancer patients (**Supplementary Figure 4B-C**).

Functional Enrichment Analysis of UROC1 in Pan-Cancer

To investigate the molecular mechanisms of UROC1 regulation in different cancers further, we carried out GO/KEGG enrichment analysis on *UROC1* in 33 types of cancer. Herein, we only present the GSEA results related to OS in five cancers (Figure 12). In HCC, *UROC1* was mainly involved in cholesterol and amino acid metabolism, fatty acid synthesis, programmed cell death, autophagy regulation, cytoplasmic DNA sensing pathways, and *Retinoic acid-inducible gene I (RIG-I)-like receptors* signaling pathways.

Correlation Between UROC1 Expression and the TME in Pan-Cancer

The connection between *UROC1* expression and the TME was assessed by combining the Immune-score and Stromal-score. The results revealed a remarkable association between *UROC1* expression and the Immune-Score in certain tumor types, including BRCA, COAD, LAML, LGG, PRAD, TGCT and SARC (Figure 13A). In BRCA, KIRC, LAML, LGG, LIHC, OV, PRAD, TGCT, THYM, and UCEC, *UROC1* expression displayed a correlation with the Stromal-Score (Figure 13B).

UROC1 is Linked with TMB, MSI, and ICP in Pan-Cancer

TME and TMB have widely recognized characteristics that are related to tumor mutation and epigenetic alterations. According to Figure 14A, there is an inverse correlation between *UROC1*

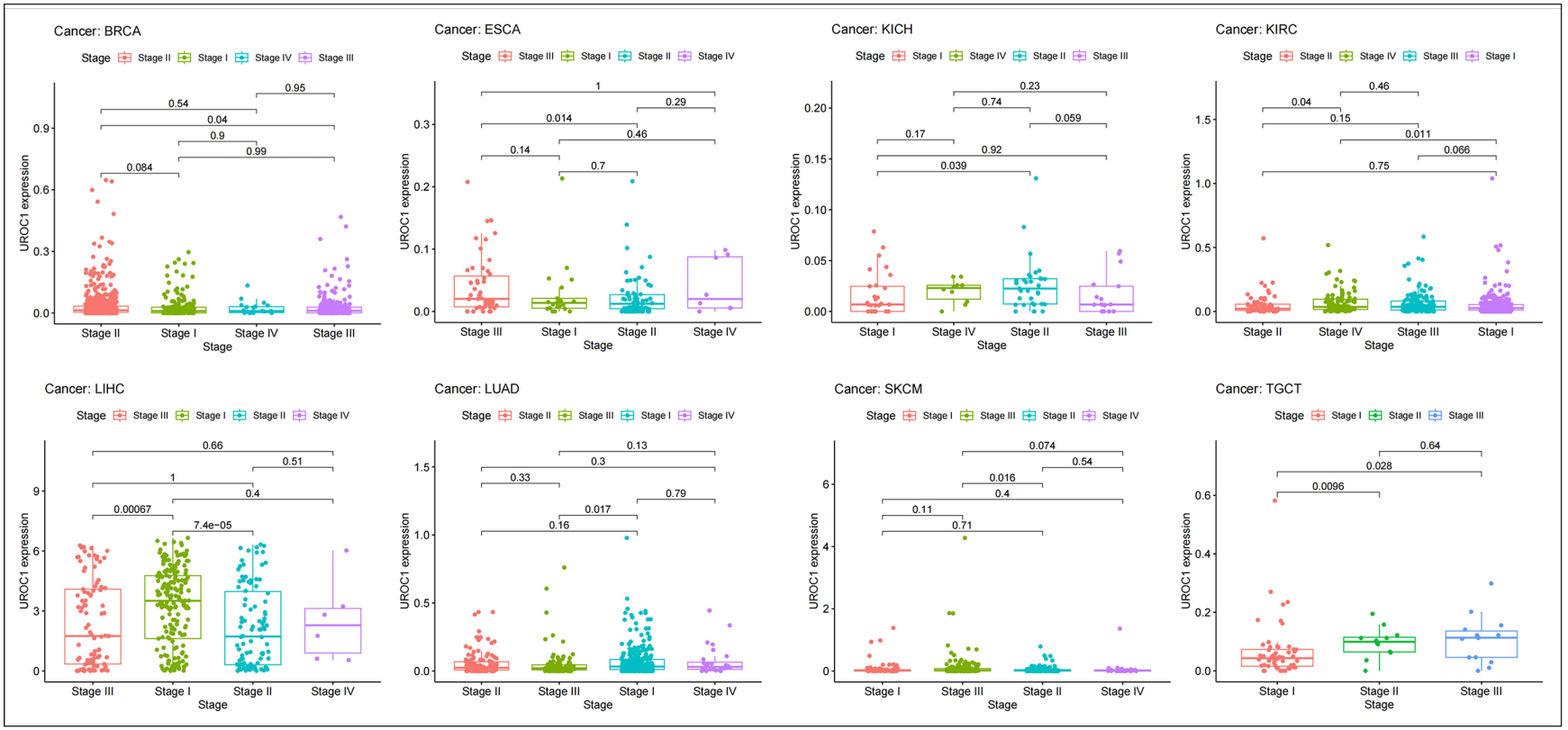

Figure 10. Association between *UROC1* expression and clinical pathological stages in pan-cancer.

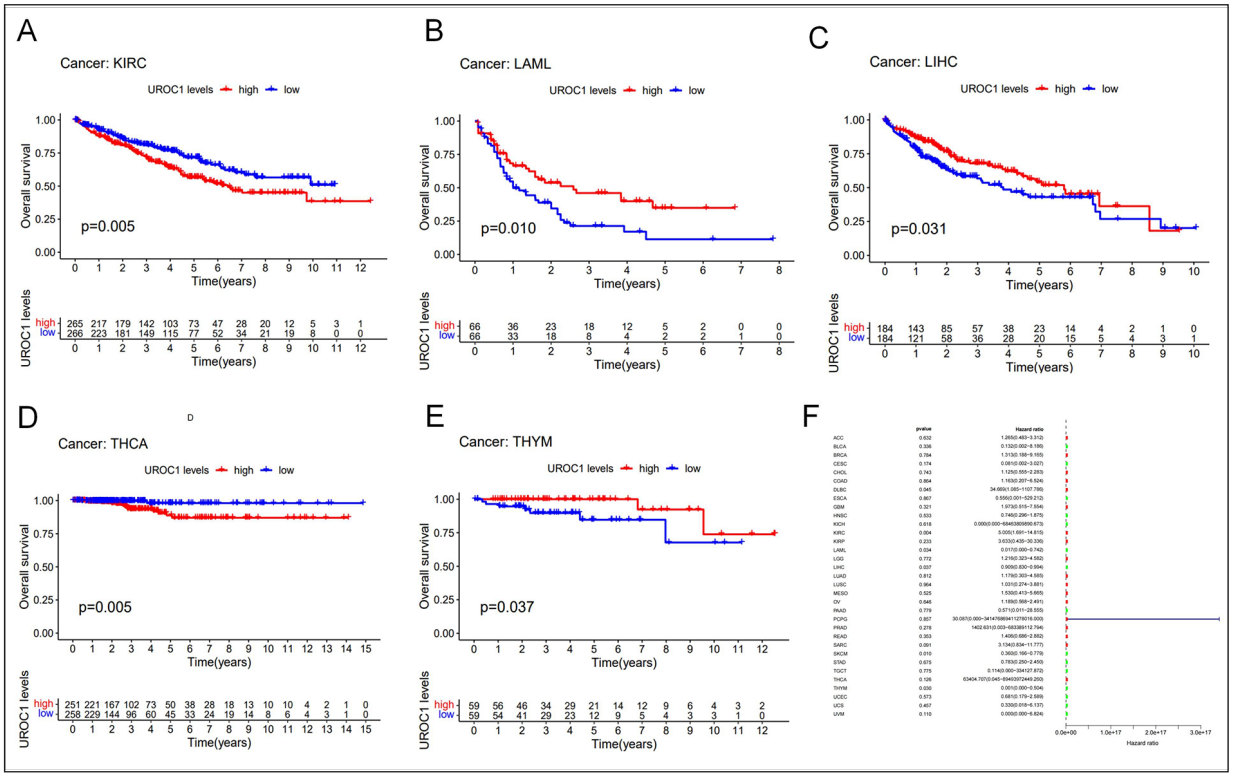

Figure 11. Association between *UROC1* expression and OS in KIRC (**A**), LAML (**B**), LIHC (**C**), THCA (**D**), THYM (**E**). **F**, Cox regression analysis.

and TMB for LUAD, THYM, and UCEC. Conversely, TGCT, LGG, BRCA, KIRC, and KIRP show a positive correlation between *UROC1* and TMB. Moving on to the relationship between *UROC1* and MSI, our findings indicate a negative relationship for UCEC and LIHC, while BRCA, SARC, PRAD, LUSC, and LGG exhibit a positive relationship (Figure 14B). Furthermore, we explored the connections between *UROC1* and 24 known ICP genes. Remarkably, our analysis revealed strong correlations between *UROC1* and the majority of ICP genes in human cancers (Figure 14C). These findings suggest that *UROC1* may play a regulatory role in tumor immunity for these types of cancers.

Validation of the Expression of UROC1 in HCC

To validate the distinct expression of *UROC1* in HCC, immunohistochemistry (IHC) was conducted. Findings revealed that compared to adjacent tissues, HCC tissues demonstrated a significant decrease in the expression level of *UROC1* (Figure 15).

Discussion

NAFLD and HCC are widely spreading diseases globally, with slow progress in the field of treatment, causing serious impacts on human health[29,30]. Therefore, seeking DEGs in NAFLD and HCC may provide new strategies to diagnose and treat patients with NAFLD/HCC. Through the intersection analysis of WGCNA, DEGs, and public databases, we identified eight HGs, including *CCL2*, *CCR2*, *IL6*, *CSF3R*, *ATL2*, *SESN3*, *UROC1*, and *FIGNL1*. Due to the differences in database selection, not all these eight genes were validated, but their roles in liver disease or other diseases have been previously reported.

Chemokine factor *CCL2* is a cytokine that coordinates the migration and localization of immune cells within tissues[31]. *CCL2* binding with *CCR2* can regulate autophagy and cell apoptosis *via* the *PIK3/Akt/mechanistic target of rapamycin complex 1 (mTORC1)* pathway or activate *JAK2*, triggering downstream signaling of *STAT5* and p38 *MAPK*, recruiting monocytes and promoting cancer cell migration and invasion leading to tumor metasta-

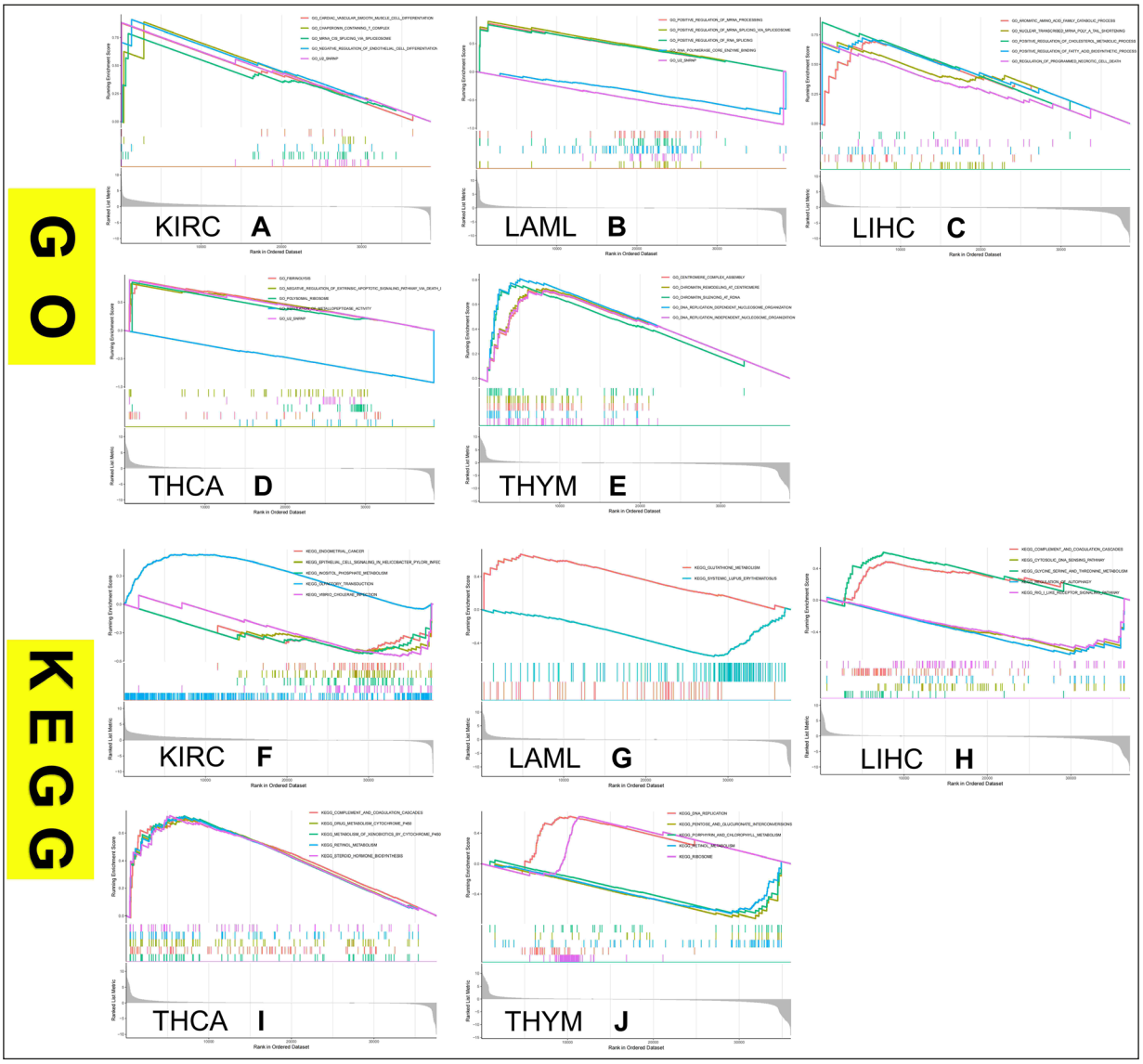

Figure 12. GO and KEGG GSEA of *UROC1* in KIRC (**A, F**), LAML (**B, G**), LIHC (**C, H**), THCA (**D, I**), THYM (**E, J**).

sis[32]. Additionally, *CCL2* can regulate cell proliferation, activation, and differentiation *via* the *TGF-β* signaling pathway and participate in nonalcoholic steatohepatitis, liver cirrhosis, and primary liver cancer[33,34].

Interleukin-6 (*IL-6*) is a type of multifunctional inflammatory cytokine, and the continuous activation of the *IL-6* is associated with HCC development[35]. By binding to its receptor, *IL-6* triggers *JAK* to activate and phosphorylate signal *STAT-3* to initiate the downstream signaling, taking part in the process of initiation, development, invasion, and metastasis of HCC cells[35,36]. Meanwhile, *IL-6* signaling can promote the production of exosomes containing microRNA-223, thus alleviating NAFLD[37].

The receptor of *granulocyte colony-stimulating factor* (*G-CSF*) is encoded by the *colony-stimulating factor 3 receptor* (*CSF3R*). Zhang et al[38] found that *GCSF* could participate in lipid metabolism and the development of NAFLD *via* the *GCSFR-suppressors of cytokine signaling 3(SOCS3)-JAK-STAT3* pathway, and insulin resistance induced by a high-fat diet was related to rat *CSF3R*[39]. Cases of HCC-producing *GCSF* have been reported[40] previously. A study[41] found that *CSF3R* is a marker of depleted CD8 T cells and can predict the response

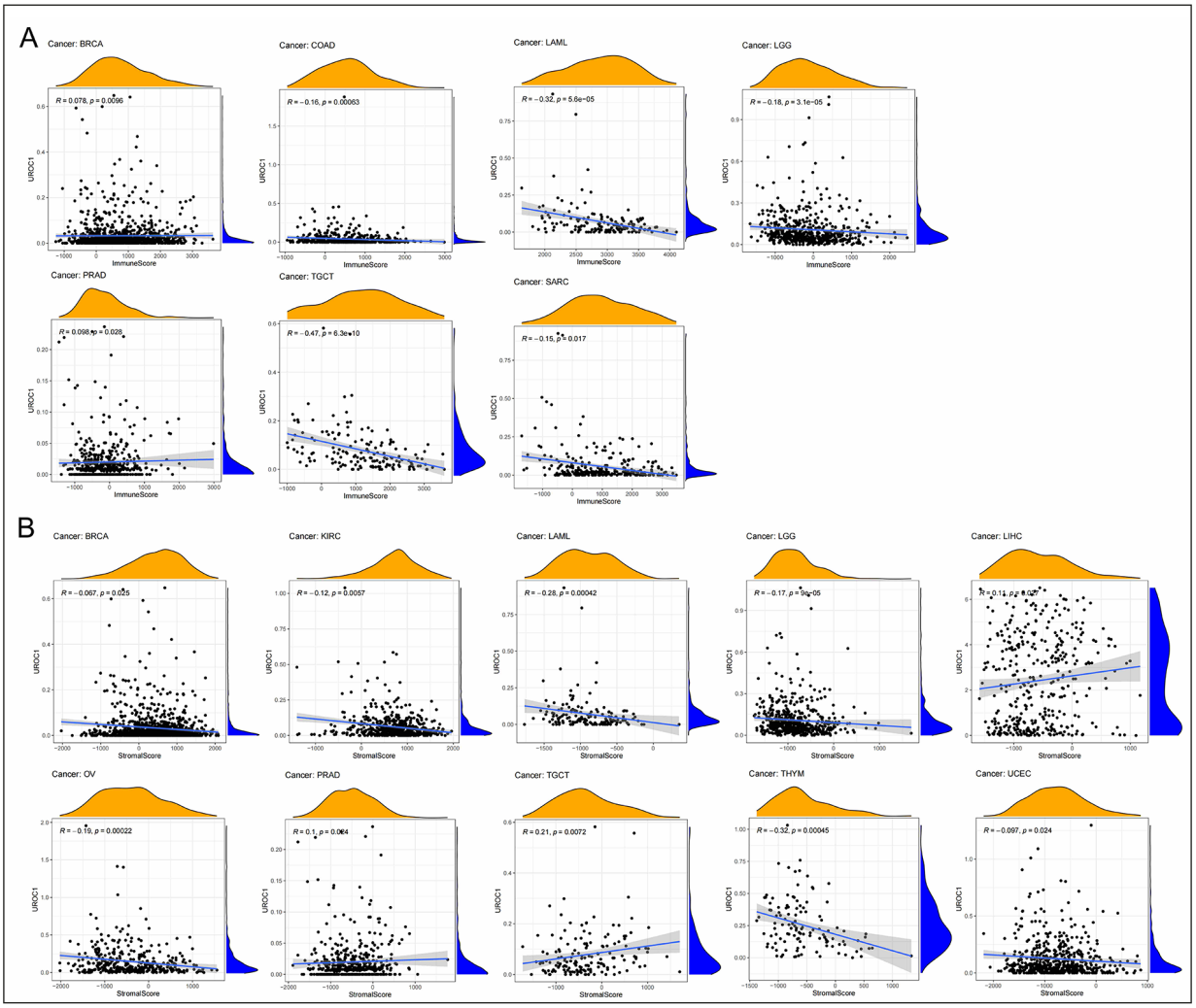

Figure 13. The relevance of *UROC1* expression to the TME. **A**, Relationship between *UROC1* expression and ImmuneScore. **B**, Relationship between *UROC1* expression and Stromal-Score.

to ICP inhibitors for HCC. New bioinformatics analysis suggests that the expression level of *GCSF* is correlated with the prognosis of HCC[42]. *GCSF* and its receptors may become a new prognostic marker for HCC, providing new strategies to diagnose and treat HCC.

*ATL*1, 2, and 3 are a class of dynamin-like GTPases localized in the endoplasmic reticulum (ER), which mediate ER membrane fusion[43]. *ATL* regulates various ER-associated processes, such as autophagy, calcium homeostasis, lipid formation, and mitochondrial function[43-46]. Additionally, it has been reported[47,48] that *ATL2* is correlated with breast and gastric cancer metastasis, but its mechanism in NAFLD/HCC remains unknown. A whole-genome association study[49] has indicated that genes such as *ATL2* play a crucial role in the regulation of adipose tissue morphology by modulating the proliferation and differentiation of precursor cells. This will help us explore the potential mechanisms underlying the interaction between *ATL2* and NAFLD/HCC.

Sestrin3 (*SESN3*) belongs to a small protein family that can act on *IL-6/STAT3* to inhibit HCC progression[50] and inhibit *TGFβ-Smad3* signaling transduction, thereby regulating extracellular matrix and liver fibrosis[51]. Furthermore, *SESN3* is crucial in NAFLD and HCC by inhibiting *SMAD3* and regulating adipocytes[52], as well as directly activating *mTORC2-Akt* signaling to enhance insulin sensitivity[53]. *Fidgetin-like 1* (*FIGNL1*) belongs to the ATPase superfamily and is involved in multiple cellular activities[54]. Zhen et al[28] revealed correlations between *FIGNL1*

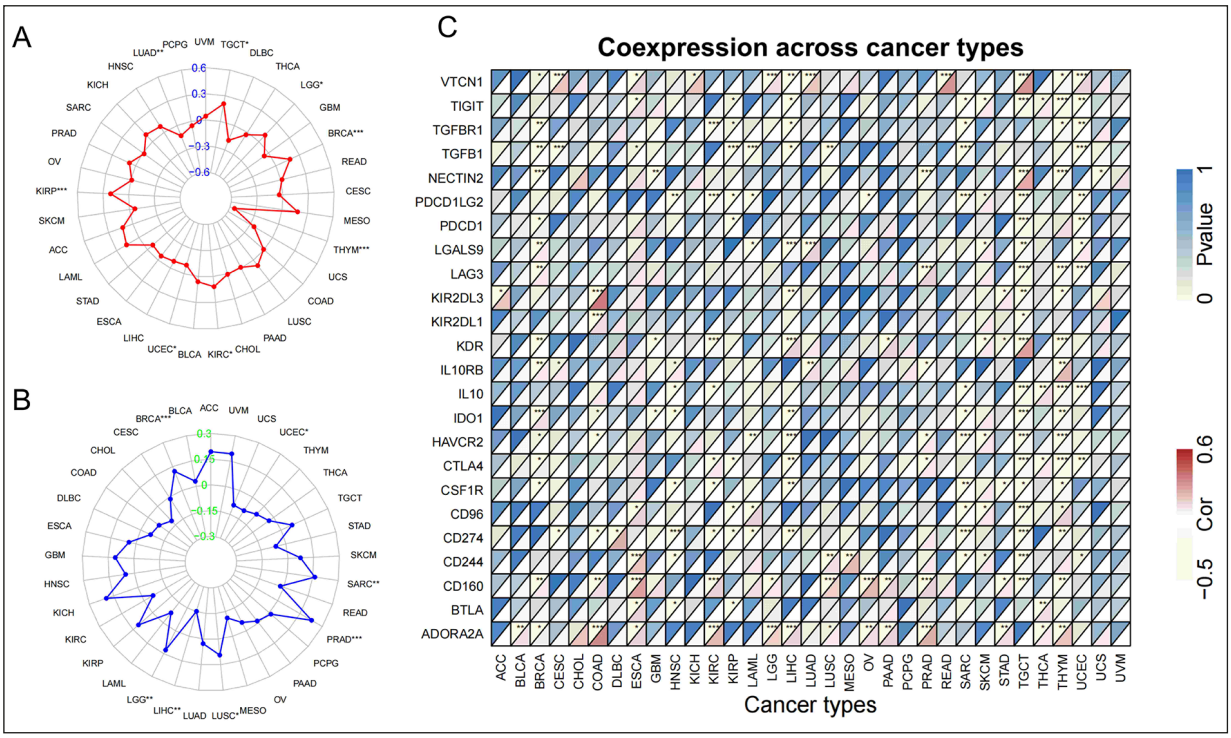

Figure 14. The correlation of *UROC1* expression with TMB, MSI, and ICP. **A**, Correlation between *UROC1* and TMB. **B**, Correlation between *UROC1* and MSI. **C**, Correlation between *UROC1* and *ICP* genes.

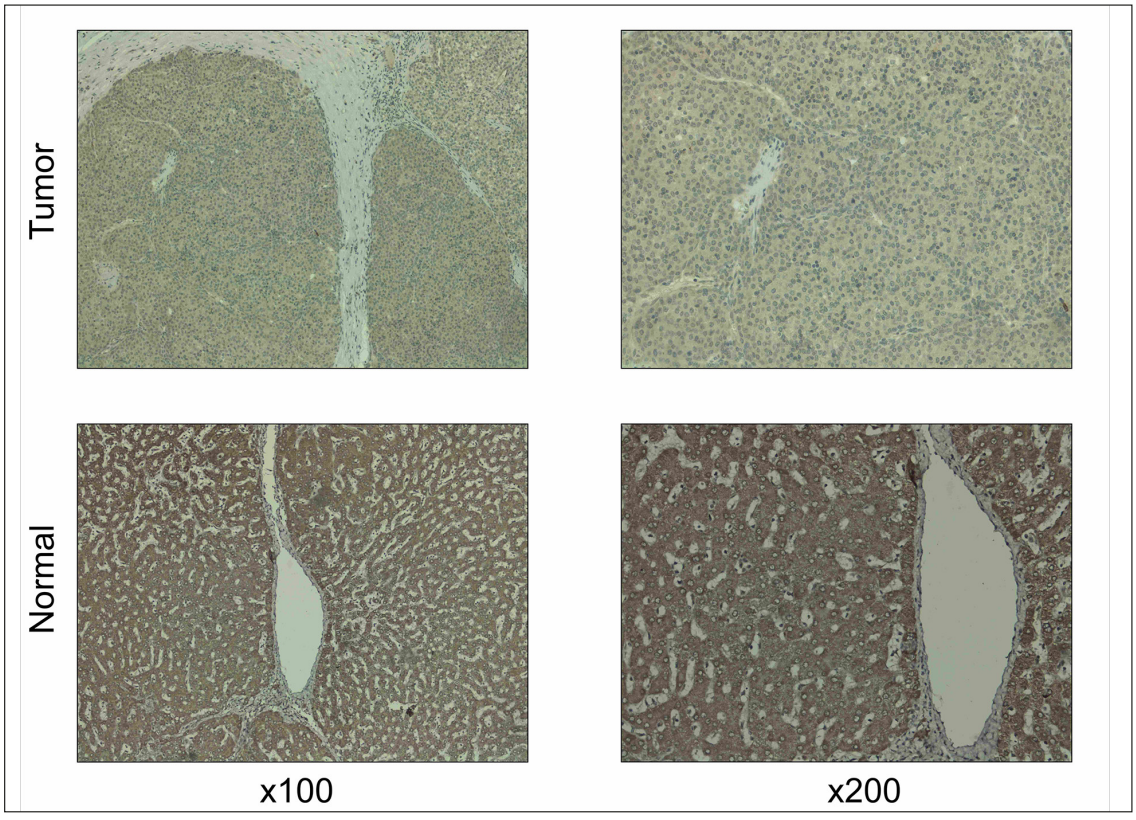

Figure 15. Representative IHC staining for *UROC1* in HCC and adjacent non-tumor tissues.

expression and LGG, KIRP, as well as LIHC prognosis, promoter methylation, and immune infiltration through pan-cancer analysis, which requires further validation.

Uricase encoded by *UROC1* catalyzes the second step of histidine degradation, resulting in the hydration of uric acid to form imidazolinone propionate[55]. In some case studies[56], uricase deficiency has been associated with intellectual disability. Zhang et al[57] found the specific key genes for alcohol-related HCC through bioinformatics analysis, including the *UROC1* gene. The study found that *UROC1* was downregulated in alcohol-related HCC, which is consistent with our observation, indicating an important role of *UROC1* in HCC, but its specific mechanism requires further research, and no other reports have been found so far.

The pathogenesis of HCC originating from NAFLD/NASH is very complex and involves various mechanisms such as inflammation, apoptosis, cell cycle, and cell death[58,59]. Immunotherapy is considered a promising approach to overcome this dilemma[60]. The liver is an immune organ with abundant immune-active cells, such as Kupffer cells (KCs), hepatic stellate cells (HSCs), natural killer cells (NKs), liver sinusoidal endothelial cells (LSECs), and lymphocytes, including Natural killer T (NKT) cells, γδT cells, and dendritic cells (DC)[61]. Immune cell activation is accompanied by the production of inflammatory and chemotactic factors such as *TNFα, IL-1β, IL-6*, and *CCL2*, exacerbating liver inflammation and damage leading to fibrosis, even progressing to cirrhosis and HCC[62]. The heterogeneity of HCC is partially explained by the characteristics of the tumor microenvironment (TME), with the innate and adaptive immune system cells being the major components[63].

In the innate immune system, KCs can be activated by *toll-like receptor (TLR)* expression induced by endotoxins, complement, and other molecular patterns that are associated with pathogens, promoting insulin resistance, inflammation, and even fibrosis in NAFLD patients[62,64,65]. In the HCC environment, KCs induce T-cell tolerance and dysfunction, thereby inhibiting anti-tumor activity[66,67]. The antigen uptake and presentation of LSEC scavenger receptors play a critical role in developing T cell tolerance under physiological circumstances. The collagen fibers and extracellular matrix components are produced by HSCs and directly participate in liver fibrosis[68,69]. NKs can inhibit liver fibrosis progression by killing the activated HSCs[70], and NKT cells are central immune participants in the progression of liver inflammation to liver fibrosis, which is related to NASH to HCC progression[71,72]. Additionally, DCs are professional antigen-presenting cells, and mature DCs not only induce anti-tumor reactive T cells but also mediate HCC immune escape by inducing tolerance to presented tumor antigens[72]. γδT cells are unconventional T lymphocytes that connect innate and adaptive immunity[73].

A growing body of evidence[74] indicates that adaptive immunity drives NAFLD progression, in which T cells play a pivotal role. CD4 T cells have multiple functional subsets, such as helper T (Th) 1, Th2, Th17, T regulatory (Treg) cells, and follicular helper T (Tfh) cells. CD8 T cells are composed of cytotoxic T cells (Tc) and CD8 Treg cells. Among them, the polarization of Th2 and Th17 responses is considered as the driving force of liver fibrosis. CD8 T cells and their helper CD4CD25-Th cells are suppressed in HCC patients, and the functional changes of these T cells promote the occurrence and development of HCC[72,74,75]. Consistent with previous reports[72,74,75], our enrichment analysis results involved Th1, Th2, and Th17 cell differentiation and multiple inflammation-related pathways. Our immune infiltration analysis also revealed the roles of different immune cells in NAFLD and HCC and their relationship with HGs. Therefore, the role of immunotherapy in NAFLD and HCC deserves our attention.

Cancer poses a significant challenge to the global population, burdening mankind with its diverse manifestations. Throughout the entire course of this illness, the immune system establishes an intricate connection with the malignant growths. Our pan-cancer analysis of *UROC1* explored the association of *UROC1* expression with the occurrence and prognosis of multiple cancers. Specifically, low expression of *UROC1* is associated with poor clinical prognosis of liver cancer, and its underlying mechanism may be related to substance metabolism, programmed cell death, and autophagy regulation. Necroptosis promotes tumor progression and invasion, and the crosstalk between necroptosis and autophagy plays a role in a variety of tumors[76]. Autophagy can affect cancer in various ways[77,78], and the role of *RIG-I*-like receptors in tumor treatment has been demonstrated[79] in liver cancer and other cancers. The immune system activation involves the participation of the DNA sensing pathway, indicating its crucial function in suppressing tumor

growth[80]. Furthermore, *UROC1* is closely related to TMB, MSI, ICP, and TME. These results further demonstrate the role of *UROC1* in carcinogenesis and tumor immunity.

Limitations

However, this study has certain limitations. Firstly, our analysis was mainly based on retrospective analysis of different databases, and all identified genes' expressions and functions require further validation in experimental studies. Moreover, the pan-cancer analysis results of *UROC1* also need more comprehensive and detailed supplementary discussions. More clinical trials are warranted to further confirm the connection between *UROC1* expression and patients' clinical features and prognosis.

Conclusions

Overall, our analysis identified several novel genes (*CCL2*, *CCR2*, *IL6*, *CSF3R*, *ATL2*, *SESN3*, *UROC1*, and *FIGNL1*) that could serve as potential biological and immunological biomarkers. This research expands our understanding of *UROC1* in the progression of malignant tumors, providing new evidence for the broad application prospects of *UROC1* in the field of HCC and other cancer research.

Conflict of Interest

The authors declare that they have no conflict of interests.

Funding

The study did not receive any specific funding from funding agencies in the public, commercial or non-profit sectors.

Authors' Contribution

Conceptualization: Qiaoyun Wang; Methodology: Qiaoyun Wang, Han Xiao; Formal analysis and investigation: Qiaoyun Wang, Yingjie Liu, Yue Hu; Writing - original draft preparation: Qiaoyun Wang; Writing review and editing: Qiaoyun Wang; Funding acquisition: Lingling Xia, Yonggui Wu; Resources: Lingling Xia, Yonggui Wu; Supervision: Lingling Xia, Yonggui Wu and all authors commented on previous versions of the manuscript. All authors read and approved the final manuscript.

Data Availability

Gene Expression Omnibus (GEO) database (http://www.ncbi.nlm.nih.gov/geo/); Comparative Toxicogenomics Database (CTD; http://ctdbase.org/); GeneCards (http://www.GeneCards.org/); DisGeNET (http://www.disgenet.org/); TCGA (https://portal.gdc.cancer.gov/).

Ethics Approval

This study was approved by the Ethics Committee of the First Affiliated Hospital of Anhui Medical University (Ethical Approval No. PJ2023-06-33).

Informed Consent

Not applicable.

ORCID ID

Qiaoyun Wang: 0009-0007-6913-7557.

References

1) Powell EE, Wong VW, Rinella M. Non-alcoholic fatty liver disease. Lancet (London, England) 2021; 397: 2212-2224.
2) Foerster F, Gairing SJ, Müller L, Galle PR. NAFLD-driven HCC: Safety and efficacy of current and emerging treatment options. J Hepatol 2022; 76: 446-457.
3) Estes C, Anstee QM, Arias-Loste MT, Bantel H, Bellentani S, Caballeria J, Colombo M, Craxi A, Crespo J, Day CP, Eguchi Y, Geier A, Kondili LA, Kroy DC, Lazarus JV, Loomba R, Manns MP, Marchesini G, Nakajima A, Negro F, Petta S, Ratziu V, Romero-Gomez M, Sanyal A, Schattenberg JM, Tacke F, Tanaka J, Trautwein C, Wei L, Zeuzem S, Razavi H. Modeling NAFLD disease burden in China, France, Germany, Italy, Japan, Spain, United Kingdom, and United States for the period 2016-2030. J Hepatol 2018; 69: 896-904.
4) Huang DQ, El-Serag HB, Loomba R. Global epidemiology of NAFLD-related HCC: trends, predictions, risk factors and prevention. Nat Rev Gastroenterol Hepatol 2021; 18: 223-238.
5) Toh MR, Wong EYT, Wong SH, Ng AWT, Loo LH, Chow PK, Ngeow J. Global Epidemiology and Genetics of Hepatocellular Carcinoma. Gastroenterology 2023; 164: 766-782.
6) Yang JD, Hainaut P, Gores GJ, Amadou A, Plymoth A, Roberts LR. A global view of hepatocellular carcinoma: trends, risk, prevention and management. Nat Rev Gastroenterol Hepatol 2019; 16: 589-604.
7) Fujiwara N, Friedman SL, Goossens N, Hoshida Y. Risk factors and prevention of hepatocellular carcinoma in the era of precision medicine. J Hepatol 2018; 68: 526-549.
8) Desai A, Sandhu S, Lai JP, Sandhu DS. Hepatocellular carcinoma in non-cirrhotic liver: A comprehensive review. World J Hepatol 2019; 11: 1-18.

9) Tovo CV, de Mattos AZ, Coral GP, Sartori GDP, Nogueira LV, Both GT, Villela-Nogueira CA, de Mattos AA. Hepatocellular carcinoma in non-alcoholic steatohepatitis without cirrhosis. World J Gastroenterol 2023; 29: 343-356.

10) Iizuka N, Oka M, Yamada-Okabe H, Nishida M, Maeda Y, Mori N, Takao T, Tamesa T, Tangoku A, Tabuchi H, Hamada K, Nakayama H, Ishitsuka H, Miyamoto T, Hirabayashi A, Uchimura S, Hamamoto Y. Oligonucleotide microarray for prediction of early intrahepatic recurrence of hepatocellular carcinoma after curative resection. Lancet (London, England) 2003; 361: 923-929.

11) Choudhary NS, Duseja A. Genetic and epigenetic disease modifiers: non-alcoholic fatty liver disease (NAFLD) and alcoholic liver disease (ALD). Transl Gastroenterol Hepatol 2021; 6: 2.

12) Liu J, Lin B, Chen Z, Deng M, Wang Y, Wang J, Chen L, Zhang Z, Xiao X, Chen C, Song Y. Identification of key pathways and genes in nonalcoholic fatty liver disease using bioinformatics analysis. Arch Med Sci 2020; 16: 374-385.

13) Cai C, Song X, Yu C. Identification of genes in hepatocellular carcinoma induced by non-alcoholic fatty liver disease. Cancer Biomark 2020; 29: 69-78.

14) Leoni S, Tovoli F, Napoli L, Serio I, Ferri S, Bolondi L. Current guidelines for the management of non-alcoholic fatty liver disease: A systematic review with comparative analysis. World J Gastroenterol 2018; 24: 3361-3373.

15) Davis AP, Grondin CJ, Johnson RJ, Sciaky D, Wiegers J, Wiegers TC, Mattingly CJ. Comparative Toxicogenomics Database (CTD): update 2021. Nucleic Acids Res 2021; 49: D1138-D1143.

16) Safran M, Dalah I, Alexander J, Rosen N, Iny Stein T, Shmoish M, Nativ N, Bahir I, Doniger T, Krug H, Sirota-Madi A, Olender T, Golan Y, Stelzer G, Harel A, Lancet D. GeneCards Version 3: the human gene integrator. Database (Oxford) 2010; 2010: baq020.

17) Piñero J, Bravo À, Queralt-Rosinach N, Gutiérrez-Sacristán A, Deu-Pons J, Centeno E, García-García J, Sanz F, Furlong LI. DisGeNET: a comprehensive platform integrating information on human disease-associated genes and variants. Nucleic Acids Res 2017; 45: D833-D839.

18) Tomczak K, Czerwińska P, Wiznerowicz M. The Cancer Genome Atlas (TCGA): an immeasurable source of knowledge. Contemp Oncol (Pozn) 2015; 19: A68-A77.

19) Goldman MJ, Craft B, Hastie M, Repečka K, McDade F, Kamath A, Banerjee A, Luo Y, Rogers D, Brooks AN, Zhu J, Haussler D. Visualizing and interpreting cancer genomics data via the Xena platform. Nat Biotechnol 2020; 38: 675-678.

20) Ritchie ME, Phipson B, Wu D, Hu Y, Law CW, Shi W, Smyth GK. limma powers differential expression analyses for RNA-sequencing and microarray studies. Nucleic Acids Res 2015; 43: e47.

21) Yu G, Wang LG, Han Y, He QY. ClusterProfiler: an R package for comparing biological themes among gene clusters. OMICS 2012; 16: 284-287.

22) von Mering C, Huynen M, Jaeggi D, Schmidt S, Bork P, Snel B. STRING: a database of predicted functional associations between proteins. Nucleic Acids Res 2003; 31: 258-261.

23) Doncheva NT, Morris JH, Gorodkin J, Jensen LJ. Cytoscape StringApp: Network Analysis and Visualization of Proteomics Data. J Proteome Res 2019; 18: 623-632.

24) Langfelder P, Horvath S. WGCNA: an R package for weighted correlation network analysis. BMC Bioinformatics 2008; 9: 559.

25) Chen T, Liu YX, Huang LJI. ImageGP: An easy-to-use data visualization web server for scientific researchers. iMeta 2022; 1: e5.

26) Newman AM, Liu CL, Green MR, Gentles AJ, Feng W, Xu Y, Hoang CD, Diehn M, Alizadeh AA. Robust enumeration of cell subsets from tissue expression profiles. Nat Methods 2015; 12: 453-457.

27) Freshour SL, Kiwala S, Cotto KC, Coffman AC, McMichael JF, Song JJ, Griffith M, Griffith OL, Wagner AH. Integration of the Drug-Gene Interaction Database (DGIdb 4.0) with open crowdsource efforts. Nucleic Acids Res 2021; 49: D1144-D1151.

28) Zhen Z, Li M, Zhong M, Ye L, Ma X. FIGNL1 Expression and its Prognostic Significance in Pan-cancer Analysis. Comb Chem High Throughput Screen 2022; 25: 2180-2190.

29) Estes C, Razavi H, Loomba R, Younossi Z, Sanyal AJ. Modeling the epidemic of nonalcoholic fatty liver disease demonstrates an exponential increase in burden of disease. Hepatology (Baltimore, Md) 2018; 67: 123-133.

30) Muthiah MD, Sanyal AJ. Current management of non-alcoholic steatohepatitis. Liver Int 2020; 40: 89-95.

31) Deshmane SL, Kremlev S, Amini S, Sawaya BE. Monocyte chemoattractant protein-1 (MCP-1): an overview. J Interferon Cytokine Res 2009; 29: 313-326.

32) She S, Ren L, Chen P, Wang M, Chen D, Wang Y, Chen H. Functional Roles of Chemokine Receptor CCR2 and Its Ligands in Liver Disease. Front Immunol 2022; 13: 812431.

33) Karlmark KR, Weiskirchen R, Zimmermann HW, Gassler N, Ginhoux F, Weber C, Merad M, Luedde T, Trautwein C, Tacke F. Hepatic recruitment of the inflammatory Gr1+ monocyte subset upon liver injury promotes hepatic fibrosis. Hepatology (Baltimore, Md) 2009; 50: 261-274.

34) Dituri F, Mancarella S, Cigliano A, Chieti A, Giannelli G. TGF-β as Multifaceted Orchestrator in HCC Progression: Signaling, EMT, Immune Microenvironment, and Novel Therapeutic Perspectives. Semin Liver Dis 2019; 39: 53-69.

35) Xu J, Lin H, Wu G, Zhu M, Li M. IL-6/STAT3 Is a Promising Therapeutic Target for Hepatocellular Carcinoma. Front Oncol 2021; 11: 760971.

36) Liu Y, Fuchs J, Li C, Lin J. IL-6, a risk factor for hepatocellular carcinoma: FLLL32 inhibits IL-6-induced STAT3 phosphorylation in human hepatocellular cancer cells. Cell cycle (Georgetown, Tex) 2010; 9: 3423-3427.

37) Hou X, Yin S, Ren R, Liu S, Yong L, Liu Y, Li Y, Zheng MH, Kunos G, Gao B, Wang H. Myeloid-Cell-Specific IL-6 Signaling Promotes MicroRNA-223-Enriched Exosome Production to Attenuate NAFLD-Associated Fibrosis. Hepatology (Baltimore, Md) 2021; 74: 116-132.

38) Zhang Y, Zhou X, Liu P, Chen X, Zhang J, Zhang H, Li S, Chen Y, Song X, Wang J, Zeng H, Zhang X, Tang C, Yu C, Li Y, Xu C. GCSF deficiency attenuates nonalcoholic fatty liver disease through regulating GCSFR-SOCS3-JAK-STAT3 pathway and immune cells infiltration. Am J Physiol Gastrointest Liver Physiol 2021; 320: G531-G542.

39) Fujimoto S, Mochizuki K, Shimada M, Hori T, Murayama Y, Ohashi N, Goda T. Insulin resistance induced by a high-fat diet is associated with the induction of genes related to leukocyte activation in rat peripheral leukocytes. Life Sci 2010; 87: 679-685.

40) Nagata H, Komatsu S, Takaki W, Okayama T, Sawabe Y, Ishii M, Kishimoto M, Otsuji E, Konosu H. Granulocyte colony-stimulating factor-producing hepatocellular carcinoma with abrupt changes. World J Clin Oncol 2016; 7: 380-386.

41) Hsu CL, Ou DL, Bai LY, Chen CW, Lin L, Huang SF, Cheng AL, Jeng YM, Hsu C. Exploring Markers of Exhausted CD8 T Cells to Predict Response to Immune Checkpoint Inhibitor Therapy for Hepatocellular Carcinoma. Liver Cancer 2021; 10: 346-359.

42) Cao H, Guo P, Wu X, Li J, Ge C, Wang S. GCSF as a Potential Molecular Target for Overall Survival of Hepatocellular Carcinoma. Comb Chem High Throughput Screen 2022; 25: 1005-1023.

43) Liu N, Zhao H, Zhao YG, Hu J, Zhang H. Atlastin 2/3 regulate ER targeting of the ULK1 complex to initiate autophagy. J Cell Biol 2021; 220: e202012091.

44) Niu L, Ma T, Yang F, Yan B, Tang X, Yin H, Wu Q, Huang Y, Yao ZP, Wang J, Guo Y, Hu J. Atlastin-mediated membrane tethering is critical for cargo mobility and exit from the endoplasmic reticulum. Proc Natl Acad Sci U S A 2019; 116: 14029-14038.

45) Klemm RW, Norton JP, Cole RA, Li CS, Park SH, Crane MM, Li L, Jin D, Boye-Doe A, Liu TY, Shibata Y, Lu H, Rapoport TA, Farese RV Jr, Blackstone C, Guo Y, Mak HY. A conserved role for atlastin GTPases in regulating lipid droplet size. Cell Rep 2013; 3: 1465-1475.

46) Han J, Park H, Maharana C, Gwon AR, Park J, Baek SH, Bae HG, Cho Y, Kim HK, Sul JH, Lee J, Kim E, Kim J, Cho Y, Park S, Palomera LF, Arumugam TV, Mattson MP, Jo DG. Alzheimer's disease-causing presenilin-1 mutations have deleterious effects on mitochondrial function. Theranostics 2021; 11: 8855-8873.

47) Le Guillou S, Laubier J, Péchoux C, Aujean E, Castille J, Leroux C, Le Provost F. Defects of the endoplasmic reticulum and changes to lipid droplet size in mammary epithelial cells due to miR-30b-5p overexpression are correlated to a reduction in Atlastin 2 expression. Biochem Biophys Res Commun 2019; 512: 283-288.

48) Zhong S, Wang J, Hou J, Zhang Q, Xu H, Hu J, Zhao J, Feng J. Circular RNA hsa_circ_0000993 inhibits metastasis of gastric cancer cells. Epigenomics 2018; 10: 1301-1313.

49) Lundbäck V, Kulyté A, Arner P, Strawbridge RJ, Dahlman I. Genome-Wide Association Study of Diabetogenic Adipose Morphology in the GENetics of Adipocyte Lipolysis (GENiAL) Cohort. Cells 2020; 9.

50) Liu Y, Kim HG, Dong E, Dong C, Huang M, Liu Y, Liangpunsakul S, Dong XC. Sesn3 deficiency promotes carcinogen-induced hepatocellular carcinoma via regulation of the hedgehog pathway. Biochim Biophys Acta Mol Basis Dis 2019; 1865: 2685-2693.

51) Huang M, Kim HG, Zhong X, Dong C, Zhang B, Fang Z, Zhang Y, Lu X, Saxena R, Liu Y, Zhang C, Liangpunsakul S, Dong XC. Sestrin 3 Protects Against Diet-Induced Nonalcoholic Steatohepatitis in Mice Through Suppression of Transforming Growth Factor β Signal Transduction. Hepatology (Baltimore, Md) 2020; 71: 76-92.

52) Lin W, Zhao J, Yan M, Li X, Yang K, Wei W, Zhang L, Chen J. SESN3 Inhibited SMAD3 to Relieve Its Suppression for MiR-124, Thus Regulating Pre-Adipocyte Adipogenesis. Genes 2021; 12: 1852.

53) Tao R, Xiong X, Liangpunsakul S, Dong XC. Sestrin 3 protein enhances hepatic insulin sensitivity by direct activation of the mTORC2-Akt signaling. Diabetes 2015; 64: 1211-1223.

54) Zhao X, Jin M, Wang M, Sun L, Hong X, Cao Y, Wang C. Fidgetin-like 1 is a ciliogenesis-inhibitory centrosome protein. Cell cycle (Georgetown, Tex) 2016; 15: 2367-2375.

55) Glinton KE, Levy HL, Kennedy AD, Pappan KL, Elsea SH. Untargeted metabolomics identifies unique though benign biochemical changes in patients with pathogenic variants in UROC1. Mol Genet Metab Rep 2019; 18: 14-18.

56) Espinós C, Pineda M, Martínez-Rubio D, Lupo V, Ormazabal A, Vilaseca MA, Spaapen LJ, Palau F, Artuch R. Mutations in the urocanase gene UROC1 are associated with urocanic aciduria. J Med Genet 2009; 46: 407-411.

57) Zhang X, Kang C, Li N, Liu X, Zhang J, Gao F, Dai L. Identification of special key genes for alcohol-related hepatocellular carcinoma through bioinformatic analysis. PeerJ 2019; 7: e6375.

58) Kanda T, Goto T, Hirotsu Y, Masuzaki R, Moriyama M, Omata M. Molecular Mechanisms: Connections between Nonalcoholic Fatty Liver Disease, Steatohepatitis and Hepatocellular Carcinoma. Int J Mol Sci 2020; 21: 1525.

59) Kim H, Lee DS, An TH, Park HJ, Kim WK, Bae KH, Oh KJ. Metabolic Spectrum of Liver Failure in Type 2 Diabetes and Obesity: From NAFLD to NASH to HCC. Int J Mol Sci 2021; 22: 4495.

60) Zhu J, Kuang J, Yang Y, Zhang L, Leng B, She R, Zou L. A Prognostic Model Based on NSUN3 Was Established to Evaluate the Prognosis and Response to Immunotherapy in Liver Hepatocellular Carcinoma. Mediators Inflamm 2023; 2023: 6645476.

61) Doherty DG. Immunity, tolerance and autoimmunity in the liver: A comprehensive review. J Autoimmun 2016; 66: 60-75.

62) Arrese M, Cabrera D, Kalergis AM, Feldstein AE. Innate Immunity and Inflammation in NAFLD/NASH. Dig Dis Sci 2016; 61: 1294-1303.

63) Milardi G, Lleo A. Tumor-Infiltrating B Lymphocytes: Promising Immunotherapeutic Targets for Primary Liver Cancer Treatment. Cancers 2023; 15: 2182.

64) Wen Y, Lambrecht J, Ju C, Tacke F. Hepatic macrophages in liver homeostasis and diseases-diversity, plasticity and therapeutic opportunities. Cell Mol Immunol 2021; 18: 45-56.

65) Elchaninov AV, Fatkhudinov TK, Vishnyakova PA, Lokhonina AV, Sukhikh GT. Phenotypical and Functional Polymorphism of Liver Resident Macrophages. Cells 2019; 8: 1032.

66) Dou L, Shi X, He X, Gao Y. Macrophage Phenotype and Function in Liver Disorder. Front Immunol 2019; 10: 3112.

67) Yeung OW, Lo CM, Ling CC, Qi X, Geng W, Li CX, Ng KT, Forbes SJ, Guan XY, Poon RT, Fan ST, Man K. Alternatively activated (M2) macrophages promote tumour growth and invasiveness in hepatocellular carcinoma. J Hepatol 2015; 62: 607-616.

68) Wilkinson AL, Qurashi M, Shetty S. The Role of Sinusoidal Endothelial Cells in the Axis of Inflammation and Cancer Within the Liver. Front Physiol 2020; 11: 990.

69) Gong Y, Yang Y. Activation of Nrf2/AREs-mediated antioxidant signalling, and suppression of profibrotic TGF-β1/Smad3 pathway: a promising therapeutic strategy for hepatic fibrosis - A review. Life Sciences 2020; 256: 117909.

70) Kalathil SG, Thanavala Y. Natural Killer Cells and T Cells in Hepatocellular Carcinoma and Viral Hepatitis: Current Status and Perspectives for Future Immunotherapeutic Approaches. Cells 2021; 10: 1332.

71) Oura K, Morishita A, Tani J, Masaki T. Tumor Immune Microenvironment and Immunosuppressive Therapy in Hepatocellular Carcinoma: A Review. Int J Mol Sci 2021; 22: 5801.

72) Lurje I, Hammerich L, Tacke F. Dendritic Cell and T Cell Crosstalk in Liver Fibrogenesis and Hepatocarcinogenesis: Implications for Prevention and Therapy of Liver Cancer. Int J Mol Sci 2020; 21: 7378.

73) Zhou QH, Wu FT, Pang LT, Zhang TB, Chen Z. Role of γδT cells in liver diseases and its relationship with intestinal microbiota. World J Gastroenterol 2020; 26: 2559-2569.

74) Sutti S, Albano E. Adaptive immunity: an emerging player in the progression of NAFLD. Nat Rev Gastroenterol Hepatol 2020; 17: 81-92.

75) Shuai Z, Leung MW, He X, Zhang W, Yang G, Leung PS, Eric Gershwin M. Adaptive immunity in the liver. Cell Mol Immunol 2016; 13: 354-368.

76) Lee SY, Ju MK, Jeon HM, Jeong EK, Lee YJ, Kim CH, Park HG, Han SI, Kang HS. Regulation of Tumor Progression by Programmed Necrosis. Oxid Med Cell Longev 2018; 2018: 3537471.

77) Levy JMM, Towers CG, Thorburn A. Targeting autophagy in cancer. Nat Rev Cancer 2017; 17: 528-542.

78) Li Q, Ni Y, Zhang L, Jiang R, Xu J, Yang H, Hu Y, Qiu J, Pu L, Tang J, Wang X. HIF-1α-induced expression of m6A reader YTHDF1 drives hypoxia-induced autophagy and malignancy of hepatocellular carcinoma by promoting ATG2A and ATG14 translation. Signal Transduct Target Ther 2021; 6: 76.

79) Jiang Y, Zhang H, Wang J, Chen J, Guo Z, Liu Y, Hua H. Exploiting RIG-I-like receptor pathway for cancer immunotherapy. J Hematol Oncol 2023; 16: 8.

80) Kwon J, Bakhoum SF. The Cytosolic DNA-Sensing cGAS-STING Pathway in Cancer. Cancer Discov 2020; 10: 26-39.